

ER lipid defects in neuropeptidergic neurons impair sleep patterns in Parkinson's disease

Jorge S. Valadas^{1,2}, Giovanni Esposito^{1,2}, Dirk Vandekerkhove^{1,2}, Katarzyna Miskiewicz^{1,2,†}, Liesbeth Deaulmerie^{1,2}, Susanna Raitano^{1,2}, Philip Seibler³, Christine Klein³ and Patrik Verstreken^{1,2,*}

¹ VIB-KU Leuven Center for Brain & Disease Research, 3000 Leuven, Belgium.

² KU Leuven, Department of Neurosciences, Leuven Brain Institute, 3000 Leuven, Belgium.

³ Institute of Neurogenetics, University of Lübeck, 23562 Lübeck, Germany.

† Current address: Universität Osnabrück, 49076 Osnabrück, Germany.

* Corresponding author & lead contact: patrik.verstreken@kuleuven.vib.be

Summary

Parkinson's disease patients report disturbed sleep patterns long before motor dysfunction. Here, in *parkin* and *pink1* models, we identify circadian rhythm and sleep pattern defects and map these to specific neuropeptidergic neurons in fly models and in hypothalamic neurons differentiated from patient iPSC. Parkin and Pink1 control the clearance of mitochondria by protein ubiquitination. While we do not observe major defects in mitochondria of mutant neuropeptidergic neurons, we do find an excess of endoplasmic reticulum-mitochondrial contacts. These excessive contact sites cause abnormal lipid trafficking that depletes phosphatidylserine from the ER and disrupts the production of neuropeptide-containing vesicles. Feeding mutant animals phosphatidylserine rescues neuropeptidergic vesicle production and acutely restores normal sleep patterns in mutant animals. Hence, sleep patterns and circadian disturbances in Parkinson's disease models are explained by excessive ER-mitochondrial contacts and blocking their formation or increasing phosphatidylserine levels rescues the defects *in vivo*.

Introduction

Parkinson's disease (PD) affects about 1% of the population older than 60 years (Lau and Breteler, 2006). While motor symptoms and loss of dopaminergic neurons are hallmarks of the disease (Braak et al., 2003), 99% of the patients report non-motor symptoms that include sleep defects, cognitive impairment, depression, olfactory loss and constipation (Munhoz et al., 2015). Many patients also suffer from type 2 diabetes mellitus (De Pablo-Fernández et al., 2017). Sleep pattern disturbances are particularly burdensome to PD patients (Politis et al., 2010) and manifest as insomnia, sleep fragmentation, REM sleep behavior disorders and loss of circadian rhythms (De Cock et al., 2008). These highly prevalent symptoms occur very early in the disease, often years prior to dopaminergic neuron loss and motor symptoms (Lee and Koh, 2015). Furthermore, dopaminergic replacement therapy in PD patients is able to significantly restore motor function, but is insufficient to rescue the non-motor symptoms of the disease including sleep pattern disturbances (Lee and Koh, 2015). This suggests that sleep defects originate from dysfunction of a distinct circuitry. However, the origin of sleep defects in PD remains elusive.

Although PD animal models have been tested for sleep coordination defects, the characteristic defects in circadian rhythmicity, disruption of REM sleep and sleep fragmentation seen in patients, are rarely observed in animal models (Fifel et al., 2016). This is probably because many PD models selectively target the dopaminergic system. Although mice treated with MPTP, rotenone, 6OHDA or deficient for vesicular monoamine transporter (VMAT) show typical dopaminergic neuron degeneration (Fifel et al., 2016), they do not present the diverse and frequent non-motor symptoms of the disease. In addition, animal models of familial PD, where specific genes are knocked out or pathogenic mutations are expressed, do not present the sleep phenotypes typical of the disease (Fifel et al., 2016). Hence, models that broadly affect the nervous system are needed to study non-motor symptoms of PD.

While PD is primarily a sporadic disease, about 10% is familial (Lill and Klein, 2015). Interestingly, both sporadic and familial PD patients display early onset sleep defects, suggesting this is fundamental

to the disease (De Cock et al., 2008; Kasten et al., 2010). Amongst PD genes, *parkin* and *pink1* are relatively well-studied and their protein products act in a common pathway to ubiquitinate mitochondrial target proteins, resulting in mitochondrial degradation (Dawson and Dawson, 2010; Valadas et al., 2015). *parkin* encodes for the E3 ubiquitin ligase that catalyzes the ubiquitination of specific targets, guiding them to degradation or to a different cellular location (Pickrell and Youle, 2015). If Parkin function is impaired, its targets accumulate in the cell. Pink1 is a kinase that activates Parkin by phosphorylation (Pickrell and Youle, 2015). Upon mitochondrial depolarization, Pink1 is stabilized on the outer mitochondrial membrane and recruits Parkin to promote the removal of damaged mitochondria (Pickrell and Youle, 2015). An expected long-term consequence of Parkin or Pink1 loss is the accumulation of dysfunctional mitochondria (Pickrell and Youle, 2015), however this is not observed in all neuronal cell types *in vivo*. In addition to causative mutations in the *parkin* gene, Parkin protein is also often inactivated in sporadic PD (Dawson and Dawson, 2010) and similar to sporadic PD, patients with *parkin* or *pink1* mutations exhibit sleep pattern defects (Kasten et al., 2010).

Parkin and Pink1 are broadly expressed in the brain (Stichel et al., 2000; Taymans et al., 2006) and in this work, we use loss of function mutations in *parkin* and *pink1* and study them both in hypothalamic neurons differentiated from patient induced pluripotent stem cells (iPSC) and in fruit flies, to dissect the molecular, cellular and neurobiological origin of the circadian and sleep pattern defects in PD. We find that excess transfer of phosphatidylserine at the ER-mitochondrial contacts of mutant neuropeptidergic neurons causes a defect to produce loaded secretory vesicles that control circadian rhythms. Increasing phosphatidylserine levels is sufficient to rescue secretory vesicle production and sleep pattern defects in the PD models.

Results

Parkinson's disease models have sleep pattern defects

The mechanisms of sleep maintenance and circadian rhythmicity control are well-conserved across species, including *Drosophila melanogaster* (Hendricks and Sehgal, 2004; Hendricks et al., 2000). Besides a higher threshold to arousal, sleeping flies do not move, and inactivity over a 5 min period is regarded as a good measure of sleep, also verified by alternative methodologies (Chiu et al., 2010; Hendricks et al., 2000). To assess features of circadian rhythmicity we used automated monitoring to continuously follow the movement of flies that lack *parkin* or *pink1* (Park et al., 2006; Pesah et al., 2004). Interestingly, several aspects of the circadian pattern are disrupted in both *parkin* and *pink1* mutants compared to controls as summarized in Figure 1A and Figure S1A-C.

Two sleep pattern features are particularly disrupted in *pink1* and *parkin* mutants and these defects are also observed in the disrupted sleep patterns of PD patients: [1] the anticipation of dawn and [2] the fragmentation of sleep (De Pablo-Fernández et al., 2017; Peeraully et al., 2012). Wild type flies kept on a 12 h dark-light cycle use their endogenous circadian rhythms to anticipate the timing of dusk or dawn, becoming more active in the 3 h period preceding these events (Figure 1A) (Chiu et al., 2010). In contrast, flies with *parkin* or *pink1* mutations fail to anticipate dawn (and to a lesser extent dusk) and remain inactive until the switch to light (Figure 1B-C). We confirm that the morning and evening anticipation defects are specific to *parkin* or *pink1* loss by analyzing different independently generated mutants (Figure S1D). In addition, the defects in morning and evening anticipation are also reversed by re-expressing wild type Parkin or Pink1, but not by re-expressing mutant forms of these proteins (Figure 1B-C and Figure S1D) (Clark et al., 2006; Pesah et al., 2004). Note that the presence of these genomic rescue constructs in a wild type background does not affect any of the measured parameters. Furthermore, we also find that *parkin* and *pink1* mutant flies show normal overall locomotor activity, ruling out that our observations are the result of decreased motor ability (Figure S1E).

To further examine this circadian defect in *parkin* and *pink1* mutants we trained the flies in 12h light-dark cycles for 7 days and then assessed the maintenance of circadian rhythmicity in the absence of a light cycle by keeping the flies in constant darkness. Despite the continuous darkness, wild type flies still display a strong circadian dependent oscillatory pattern with a bout of activity at dusk and dawn. In contrast, *parkin* and *pink1* mutants have a weaker oscillatory amplitude (Figure S1F,G). The circadian period, which is a direct measurement of the coordinated expression and degradation of the circadian genes and proteins (*period*, *clock*, etc.), is not altered in flies with *parkin* or *pink1* mutations (Figure 1D); however, we detect a significant decrease in the number of rhythmic flies (Figure 1E) and a loss of the circadian power (Figure 1F). These results implicate Parkin and Pink1 in the control of endogenous circadian rhythmicity through a mechanism independent of the regulation of the circadian genes.

Another prominent feature observed in PD patients is an inability to maintain sleep, manifested as sleep fragmentation during the night (Peeraully et al., 2012). As noted above, we find frequent awakenings (short periods of activity that are preceded and succeeded by a sleep period) in *parkin* and *pink1* mutant flies and these occur both during the night and day (Figure 1G, I-J and Figure S2A-D). Again, we rescue these defects by re-expressing wild type Parkin or Pink1 (Figure 1G, I-J and Figure S2A-D). The sleep fragmentation is the result of a decrease in the length of the sleep bouts and an increase in their frequency (Figure S2E-H). While *parkin* and *pink1* mutant flies display fragmented sleep, similar to patients, their total amount of sleeping minutes (at night or during the day) is not affected (Figure 1H and Figure S2I-L). We conclude that *pink1* and *parkin* mutant flies recapitulate several cardinal features of rhythmicity and sleep pattern disturbances that are also evident in PD.

Neuropeptidergic neuron defects in *parkin* and *pink1* mutants

To define the cells responsible for the circadian rhythmicity and sleep pattern defects, we resorted to cell type specific *parkin*^{RNAi} expression. We first show that *parkin*^{RNAi} or *pink1*^{RNAi} expression

significantly lower *parkin* or *pink1* RNA expression (Figure S2M). Organism-wide or neuron-specific *parkin*^{RNAi} and *pink1*^{RNAi} expression (Tubulin-Gal4 or Elav-Gal4) both recapitulate the morning anticipation and brief awakening defects observed in *parkin* and *pink1* null mutants (Figure 2A,B), indicating that Parkin and Pink1 control these via a role in neurons. We further refined the defect by mapping them to specific neuronal clusters in the brain using GAL4-mediated expression of the RNAi construct in different circadian and sleep-related neuronal clusters. *parkin*^{RNAi} or *pink1*^{RNAi} mimic specific aspects of *parkin* and *pink1* null mutants when expressed in defined neuropeptidergic neurons (PDF-Gal4, sNPF-Gal4, Ilp2-Gal4, c929-Gal4, Figure 2A,B). In particular, RNAi expression in the ventral lateral neurons (LNv; driven by PDF-Gal4; Figure 2A,B (Renn et al., 1999)) prevents anticipation of dawn, while RNAi in Insulin Producing Cells (IPC; driven by Ilp2-Gal4 (Crocker et al., 2010)) increases the number of brief awakenings (Figure 2A,B). Indicating specificity, we find very similar results by expressing two independently generated *parkin* and *pink1* RNAi lines (Figure S2N). Our observations are in line with models of how these neurons regulate the circadian cycle (LNv) (Helfrich-Förster and Homberg, 1993; Renn et al., 1999) or sleep maintenance (IPC) (Crocker et al., 2010). Indeed, we confirm that genetic ablation of the neurons using UAS-hid or UAS-ricin also results in decreased morning anticipation (ablation of LNv) and increased brief awakenings (ablation of IPC; Figure S2O,P). Hence, loss of Parkin or Pink1 function in specific neuropeptidergic neurons is sufficient to recapitulate aspects of the circadian and sleep pattern defects.

To determine if Parkin or Pink1 function in the LNv neurons alone is sufficient to support normal morning anticipation we removed Parkin or Pink1 function everywhere except in LNv neurons. We used Tubulin-Gal4 to express RNAi in all cells, but inhibited Gal4 activity in LNv neurons by expressing Gal80 (PDF-Gal80, Figure 2C) (Stoleru et al., 2004). *parkin*^{RNAi} or *pink1*^{RNAi} expressing flies (using Tubulin-Gal4) show a defect in morning anticipation and increased brief awakenings (Figure 2D), but in the presence of PDF-Gal80, the morning anticipation defect is rescued (Figure 2D). As expected, the increased brief awakenings persist in the presence of PDF-Gal80, again indicating that this defect is elicited by the loss of Parkin or Pink1 in other cells than the LNv (e.g. IPC, Figure

2E). These results also imply that Pink1 and Parkin elicit morning anticipation defects independent of dopaminergic neuron dysfunction. We confirm this by expression of *parkin*^{RNAi} or *pink1*^{RNAi} using the dopaminergic driver ple-Gal4 and find it does not affect the morning anticipation score (Fig2A,B). This indicates morning anticipation is independent of Pink1 and Parkin function in dopaminergic cells. Conversely, we do observe a defect in brief awakenings upon *parkin*^{RNAi} expression (but not upon *pink1*^{RNAi} expression) using ple-Gal4 (Fig2A,B). This is consistent with the idea that, in addition to its role in IPC, Parkin function in dopaminergic circuits may regulate this phenotype. Nonetheless, our results indicate that Pink1 and Parkin are required in specific neuropeptidergic neurons to control circadian rhythms and sleep patterns.

Neuropeptides are arrested in neuronal cell bodies of *parkin* and *pink1* mutant flies and patient induced neurons.

We first looked at LNV neurons in more detail because knock down of Parkin or Pink1 in these neurons causes strong phenotypes in morning anticipation score. In addition, prior studies indicated that Parkin RNA levels in LNV neurons are enriched 12-fold over other neurons in the fly brain (Kula-Eversole et al., 2010). Finally, Parkin and Pink1 mRNA levels oscillate with the circadian cycle, being higher at night (Kula-Eversole et al., 2010), when the LNV neurons actively release Pigment Dispersing Factor (PDF). We therefore assessed if *parkin* and *pink1* mutant LNV neurons produce PDF-loaded vesicles and transport these to the terminals. We labelled mutant brains at *Zeitgeber* Time 23 (1 hour before the lights on event) with anti-PDF antibody (Figure 3A). This finds reduced levels of PDF at neuron terminals and increased PDF levels in cell bodies compared to controls (Figure 3B-C). These differences are not because of changes in PDF mRNA expression levels in the mutants as gauged by qPCR (Figure S3A). Furthermore, the PDF distribution defects are recapitulated by RNAi-mediated downregulation of Parkin or Pink1 in LNV neurons, indicating the effect is cell autonomous to these neuropeptidergic neurons (Figure S3B-E).

Next, we analyzed the defects underlying the brief awakenings phenotype that was strongly affected in *pink1* and *parkin* mutants. Loss of Pink1 and Parkin in several neuropeptidergic neuron clusters and the loss of Parkin in the dopaminergic neurons affected this parameter (Figure 2A,B). We chose to analyze neuropeptide distribution in the IPC, because of their concentrated, specific localization in the brain (Figure 3A') and because we have access to specific antibodies that recognize insulin-like peptide type 2 (dIlp2), produced in the IPC (Rulifson et al., 2002). We find dIlp2 labeling is increased in the IPC cell bodies and decreased in the IPC neuron terminals (Figure 2D-E). Hence, both dIlp2 (in the IPC) and PDF (in the LNV) fail to properly localize at terminals and are retained in the cell body.

To further test the neuropeptide distribution defects, we expressed an exogenous neuropeptide, rat neuropeptide Atrial Natriuretic Factor tagged with GFP (ANF-GFP) (Rao et al., 2001) in the LNV or IPC. ANF uses the fly cellular machinery to be produced and processed and we find it is also retained in the cell bodies of the LNV (Figure S3F) and of the IPC (Figure S3G) of *parkin* mutant flies. Finally, the defect we observe is specific to neuropeptides because expression of Synaptotagmin-GFP, a synaptic vesicle associated protein also produced in the cell body, distributes normally to synapses of LNV neurons in the mutants (Figure S3H,I). These data indicate that neuropeptide distribution is broadly affected in Parkinson's disease mutant flies.

Fly LNV neurons are analogous to neurons in the human hypothalamus and both fly and human neurons secrete neuropeptides in the hours preceding dawn (Kunst et al., 2015; Richter et al., 2014). Human neurons secrete Vasoactive Intestinal Peptide (VIP), while fly neurons secrete the VIP-like neuropeptide PDF (Vosko et al., 2007). To determine if our findings are evolutionary conserved, we generated induced human hypothalamic neurons (Figure S4A) (Merkle et al., 2015). We used two patient-derived induced pluripotent stem cells (iPSC) carrying *parkin* mutations, two patients with *pink1* mutations and two age-matched individuals without PD (Figure S4B) (Seibler et al., 2011; Zanon et al., 2017). We confirmed that these four patients suffered from sleep disturbances, while the control individuals had no complaints (Figure S4B). Differentiated hypothalamic neurons with or without

parkin and *pink1* mutations express mature neuronal markers and neuropeptides, including VIP, a circadian coordinator in mammals (Figure 4A and Figure S4C). Similar to the observations in flies, we find that anti-VIP immunoreactivity is lower in neurites and increased in cell bodies of the neurons derived from the four patients (Figure 4B,C). Consistently, ELISA-based measurements of extracellular VIP show that the induced hypothalamic neurons from these patients also secrete less VIP into the medium than control cells when the neurons are chemically stimulated (Figure 4D). Hence, VIP delivery to synapses in *parkin* or *pink1* mutant human neurons is impaired also causing a defect in the coordinated release of this neuropeptide.

Neuropeptides are arrested in the ER of PD mutant neuropeptidergic cells

Neuropeptides are produced in the endoplasmic reticulum (ER), then transported through the Golgi network and loaded in DCVs that are finally transported to the release sites. The increased labelling of neuropeptides in the cell body of *parkin* or *pink1* mutant neurons can be explained either by a defect in trafficking of DCVs to their release sites, resulting in the accumulation of DCVs in cell bodies, or by the retention of neuropeptides in the ER-Golgi complex, e.g. as a result of a defect to produce DCVs.

To analyze DCV number and location in LNV neurons in the brain, we used correlative 3D Block face scanning electron microscopy. We labelled LNV neurons with anti-PDF antibody coupled to horseradish peroxidase (HRP) that converts DAB into a precipitate visible by EM (Figure S5A-D). Cell bodies of LNV neurons were then reconstructed and DCVs were identified based on morphology. The number of DCVs is significantly lower in cell bodies of *parkin* mutants (Figure 5A, and Figure S5E). Hence, despite the increased levels of PDF in *parkin* mutant LNV cell bodies, we find less DCVs. These data are consistent with a requirement for Parkin in the production of DCVs.

Neuropeptide packaging and trafficking is coupled to their post-translational processing while they transfer from the ER to the Golgi into DCVs (Loh, 1987). To directly assess neuropeptide processing we expressed dIlp2-GFP in the IPC neurons and performed western blotting to detect immature and

mature forms of dIlp2 (the GFP moiety facilitates detection on western blotting). dIlp2-GFP is produced as an immature pre-pro-neuropeptide in the ER, and is then consecutively cleaved by the fly machinery to the fully processed form that resides in DCVs (Arvan and Castle, 1998; Brogiolo et al., 2001). Consistent with our observation of decreased DCV number *parkin* mutants, we find a significant accumulation of immature uncleaved dIlp2-GFP (approx. 42kDa) and a decrease in the partially (approx. 39kDa) and fully processed dIlp2-GFP (approx. 31kDa, Figure 5C,D). We independently confirm this result by expressing ANF-GFP in *parkin* mutants where we also observe an increased amount of unprocessed and partially processed ANF-GFP at the expense of the fully processed form (Fig S5F,G) (Rao et al., 2001). These data are consistent with reduced DCV formation in *parkin* mutants.

Increased ER-mitochondrial contacts in *parkin* and *pink1* mutant neuropeptidergic neurons.

We next wondered how the function of Parkin and Pink1 could connect to DCV formation. Pink1 recruits Parkin to mitochondria where it ubiquitinates proteins (Geisler et al., 2010). In some cell types, the loss of *parkin* or *pink1* results in morphologically abnormal mitochondria (Esposito et al., 2013; Pesah et al., 2004). However, in many other cell types, including several types of neurons in flies, mice and patients, chronic loss of *parkin* and *pink1* does not cause overt mitochondrial morphological defects (Burman et al., 2012; Clark et al., 2006; Damiano et al., 2014; Gautier et al., 2008; Morais et al., 2009; Pickrell and Youle, 2015). We therefore labeled mitochondria by expressing mito-GFP in LNV neurons or with an antibody targeting TOM20 in human hypothalamic neurons with *parkin* or *pink1* mutations. This did not reveal significant changes in mitochondrial volume or mitochondrial morphology between the mutant cells and control cells (Figure S5H-J). We also assessed mitochondrial morphology in LNV neurons using electron microscopy. This does not reveal obvious abnormalities in cristae structure in the LNV of *parkin* mutants (Figure S5K).

Proteins ubiquitinated by Parkin are typically sent for degradation and an inability to ubiquitinate them, leads to elevated levels of these Parkin-targets both in *parkin* and *pink1* mutants. This has been observed for Mitofusin (*Drosophila* MARF), VDAC (*Drosophila* Porin) and Miro (Geisler et al., 2010; Poole et al., 2010; Wang et al., 2011). Interestingly, several of these targets are proteins that stabilize ER-mitochondrial contact sites (Figure S6A) (de Brito and Scorrano, 2008; Erpapazoglou and Corti, 2015; Helle et al., 2013; Poston et al., 2013). Consistently, the loss of *parkin* has been shown to result in more ER-mitochondrial contacts (Celardo et al., 2016; Gautier et al., 2016), but this was not tested in LNV neurons *in vivo*. We imaged fluorescently labelled ER and mitochondria in LNV and IPC cell bodies to evaluate the distance distribution between these organelles (see methods). This analysis indeed finds a significant increase in the contact surface between these organelles in LNV and IPC of *parkin* and *pink1* mutants (Figure 6A-D, Figure S6B-C). Similarly, we also find an increase in the ER-mitochondrial contact surface when we overexpress the Parkin target MARF in LNV neurons, indicating that the upregulation of Parkin targets is sufficient to generate more contacts (Figure S6D). We independently confirm the contact surface is increased based on volume reconstructions of our 3D EM data stacks of *parkin* mutant LNV neuron cell bodies where we highlight areas where ER and mitochondria are within a distance of <30 nm in yellow (Figure 6E). These data indicate that the loss of Parkin activity promotes the formation of ER-mitochondrial contacts in fly LNV neurons.

To determine if the increased ER-mitochondrial contact surface is evolutionary conserved, we resorted to our induced hypothalamic neurons differentiated from patient iPSC. We used antibodies to label ER (anti-PDI) and mitochondria (anti-TOM20) and also find an increased contact surface between ER and mitochondria in mutant neurons (Figure 6F-G, Figure S6E). Hence, both in mutant fly LNV and IPC, as well as in induced neuropeptidergic neurons from PD patients, the contact surface between ER and mitochondria is increased.

Increased ER-mitochondrial contacts cause morning anticipation defects in *Drosophila*

Our data suggest that defects to produce PDF-loaded DCVs in the ER-Golgi system cause circadian defects. We therefore determined if the increased ER-mitochondria contacts we observe in *parkin* and *pink1* mutants are causal to morning anticipation defects. We started by overexpressing MARF (or Porin) in LNv neurons of wild type flies where ER-mitochondrial contacts are increased (Figure S6D). This causes PDF retention in cell bodies and decreases morning anticipation, very similar to our observations in *parkin* or *pink1* mutants (Figure 7A-B, Figure S7A-B). Similarly, when we express ANF-GFP that marks DCVs and colocalizes with PDF (Figure S7J) in the flies that overexpress MARF or Porin, the ANF-GFP accumulates in LNv cell bodies at the expense of localizing to terminals (Figure 7C, Figure S7C-D). Conversely, we knocked down the Parkin target MARF (Figure S7I) in *parkin* or *pink1* mutants and find this partially rescues the PDF accumulation in the cell body as well as the defect in morning anticipation (Figure 7D-F, Figure S7E-H). Our attempts to also test another target (Porin) failed as we were unable to generate the flies. These genetic interactions are consistent with increased ER-mitochondrial contacts to cause the circadian defects we observed in *parkin* and *pink1* mutants.

To provide further evidence for a specific role of ER-mitochondrial contact sites in the regulation of morning anticipation, we created transgenic flies that express “ChiMERA” where ER-mitochondrial contacts are upregulated without the confounding factors that may arise from overexpression of endogenous proteins such as MARF or Porin. The ChiMERA protein consists of the yeast TOM70 mitochondrial membrane protein fused to the yeast ER protein, Ubc6, and GFP (Figure 7G and Figure S7K-L) (Kornmann et al., 2009). Similar to the overexpression of MARF or Porin, this tool drives ER-mitochondrial contact formation (Kornmann et al., 2009). Interestingly, expression of ChiMERA in LNv neurons causes a decrease in morning anticipation (Figure 7H). Furthermore, expression of ChiMERA results in the increased retention of PDF in LNv cell bodies and in lower levels of this neuropeptide in the LNv terminals (Figure 7I, Figure S7M-N). Hence, ER-mitochondrial contacts drive circadian rhythm defects similar to those observed in PD models.

Excessive phosphatidylserine transfer at ER-mitochondrial contacts cause circadian rhythm and sleep pattern phenotypes in *parkin* and *pink1* mutants.

ER-mitochondrial contacts are involved in different cellular processes such as Ca^{2+} export from ER to mitochondria, generation of autophagic membranes, facilitation of the ER stress response, regulation of apoptosis and also the transport of phosphatidylserine (PtdSer) from the ER to mitochondria, where it is metabolized to phosphatidylethanolamine (PtdEtn, Figure S8A, (Area-Gomez, 2014; Paillusson et al., 2016)). While we did not find evidence for a role of ER-Calcium and stress in the generation of DCVs in the literature, PtdSer has been reported to be enriched in DCV membranes (Kim et al., 2014; Westhead, 1987). Based on this, we hypothesized that the increased ER-mitochondrial contact sites in the PD mutants affect DCV production via effects on lipid membrane composition, without excluding potential other ER-related processes that may be at play as well.

To examine the lipidome of ER/Golgi- and mitochondria-enriched membranes purified from *parkin* mutants and controls, we used shotgun lipidomics. Our mitochondria-enriched fraction presents high levels of the mitochondria-resident protein ATP synthase, while the ER/Golgi-enriched fraction has high levels of Calreticulin, a protein in the ER lumen (Figure S8B,C). Both fractions only have residual levels of DLG, a postsynaptic marker (Figure S8C), indicating that our fractions are relatively pure. The protein-to-lipid ratio and the mitochondrial and ER/Golgi concentrations of phosphatidylcholine (PtdCho) are similar in controls and mutants (Figure 8A and Figure S8D). However, the mitochondrial fraction of *parkin* mutants contains significantly more PtdSer and PtdEtn than the mitochondrial fraction of controls, while the ER fraction of *parkin* mutants contains comparatively less PtdSer and PtdEtn than the ER fraction of controls (Figure 8A). This is in accordance with the increased ER-mitochondria contacts that facilitate the transfer of PtdSer from ER to mitochondria in *parkin* mutants. Mitochondrial enzymes then convert PtdSer to PtdEtn and this creates a “PtdSer sink”.

We independently confirmed the importance of ER-mitochondrial contacts to deplete PtdSer from ER by expressing ChiMERA in otherwise wild type flies. This manipulation is sufficient to drive a similar

lipid profile to the one we detect in *parkin* mutants (Figure 8A), further indicating that an increase in ER-mitochondrial contacts is sufficient to cause the lipid distribution defects in *parkin* mutants. Thus, the data indicate that increased ER-mitochondrial contacts in *parkin* mutants or in ChiMERA expressing flies, mediate excess PtdSer transfer to mitochondria, and the relative depletion of PtdSer from the ER.

Next, we tested if PtdSer levels can affect circadian rhythms. We knocked down the ER-resident enzyme PtdSer synthase with RNAi in LNV neurons (Figure S8E) and find that this manipulation causes a retention of PDF in the LNV cell bodies and a reduction of this neuropeptide at the terminals (Figure 8B, Figure S8F-G). Furthermore, knocking down PtdSer synthase also is sufficient to cause a defect in morning anticipation (Figure 8C) that is similar to that in *parkin* mutants. These data provide further evidence that a decrease in PtdSer levels in the ER/Golgi of *parkin* mutants can explain the phenotype we observe.

To test our model further we also performed a rescue experiment and supplemented fly food with PtdSer. After three days of continued PtdSer feeding, the circadian and sleep defects of *parkin* and *pink1* mutants improved; both morning anticipation (Figure 8D) and brief awakenings (Figure S8H). Furthermore, after 4 days of PtdSer feeding, the altered distribution of PDF and ANF-GFP in the LNV neurons of these *parkin* mutants is indistinguishable from the distribution we observe in controls fed or not fed with PtdSer (Figure 7E-F and Figure S8I-L). Similarly, Ilp2 distribution in the IPC neurons of *parkin* mutants fed with PtdSer is also rescued to control levels (Figure S8M-N). As a control, we also fed *parkin* and *pink1* mutants with PtdCho. However, here we do not observe a rescue of brief awakenings or morning anticipation defects (Figure S8O-P). This result indicates PtdSer depletion specifically is the basis of the circadian and sleep pattern defects in *parkin* and *pink1* mutants.

Discussion

Our data provide neurobiological, cellular and molecular explanations for circadian and sleep pattern impairments in PD – a clinically well-recognized but mechanistically not understood phenomena. The data here show that the well-known mitochondrial PD pathology in some of the genetic forms of the disease bifurcates in the cell at the level of the ER-mitochondrial contacts to affect other organelles like DCVs. These ER-mitochondrial contacts are central in aspects of lipid metabolism and we find here that the lack of PtdSer, for not yet fully clarified reasons, affects the maturation of dense core vesicles in induced neurons from patients and in fly mutants.

It is a conundrum why the manifestation of phenotypes in neurodegenerative diseases caused by mutations in a single gene do not follow simply the level of the affected protein expression i.e. not all cells respond in the same way to the presence of a mutated protein. Our data here suggest that understanding the basic cell biology is key: proteins express their function in the context of cells. We find that *parkin* and *pink1* mutations in a set of neuropeptidergic neurons affect the boost of VIP secretion that needs to happen in the hours preceding dawn, and possibly other peptides important for sleep pattern regulation as well. In fact, our mini-screen showed that knock down of Parkin or Pink1 in other neuronal clusters also elicited sleep pattern phenotypes, sometimes even in opposite directions (e.g. DH31, Tdc2 or c316), but further work will be needed to elucidate their roles in the regulation of this process. Nonetheless, our data are consistent with the normal, basal DCV production to occur normally in these cells, but the massive and fast upregulation of DCV production that is required in a limited time-window (at night) is impaired. It is clear that the particular function of these neurons makes them vulnerable to a, at a first glance relatively mild, deficit in lipid metabolism that affects DCV formation. It is likely that this stabilization of ER-mitochondrial contacts may have different consequences for other cell types, and further work is needed to evaluate to what extent this alteration might activate other pathogenic stress pathways.

Sleep pattern and circadian defects and other non-motor symptoms of PD are relatively understudied compared to the dopaminergic neuron loss and concomitant motoric defects (Munhoz et al., 2015). Part of the reason may be that murine models of familial and sporadic PD do not recapitulate the sleep pattern defects seen in patients (Fifel et al., 2016). We also tested *pink1* mutant mice using 24 h activity monitoring, but failed to detect consistent defects. We resorted to fruit flies that do recapitulate cardinal features of sleep pattern and circadian disturbances in PD. We believe this is warranted because we were able to recapitulate all the cellular defects seen in fly neuropeptidergic neurons, also in induced hypothalamic neurons from different patients that we show also display sleep defects. Moreover, the cellular and molecular substrates that regulate circadian rhythmicity and the mechanisms of sleep are evolutionary well-conserved and several aspects were originally discovered in flies (Hendricks and Sehgal, 2004).

A growing number of pathologies feature excess ER-mitochondrial contacts, for instance familial Alzheimer's disease (AD), Amyotrophic lateral sclerosis (ALS), Huntington's disease (HD) and type 2 diabetes mellitus (Krols et al., 2016). Interestingly, as in Parkinson's disease, also AD, ALS and HD have marked and penetrant sleep pattern and circadian rhythmicity symptoms (Ahmed et al., 2016; Morton, 2013; Peter-Derex et al., 2015). However, little is known about the defective cellular and molecular mechanisms at the basis of these sleep pattern defects in these different neurodegenerative diseases. Our study now provides a new direction that can be tested in the context of those diseases as well, by evaluating the processing and release of sleep pattern controlling neuropeptides. In this context our findings are exciting, because it is known that ER-mitochondrial contacts in other cell types than neuropeptidergic neurons can adapt quickly to the needs of the cell (Prudent et al., 2015). Our work suggests that through its ubiquitination activity, Parkin can "quickly" regulate the prevalence of these sites in neuropeptidergic neurons as well, as to support the boost in DCV production needed at the hours preceding dawn.

Our findings have important clinical implications. Most importantly, the circadian and sleep pattern defects in Parkinson's disease are apparently caused -at least in part- by a different pharmacology than dopaminergic dysfunction, which underlies the well-known motoric dysfunction. Indeed, sleep dysfunction in Parkinson's disease is not rescued by dopamine replacement therapy (Lee and Koh, 2015). In addition, our genetic work is in further support of this as we show that when *parkin* or *pink1* are knocked down everywhere (also in the dopaminergic neurons), except in the LNV neurons, such animals do not show a defect in morning anticipation. It is also important to note that the disordered circadian rhythmicity and sleep patterns are caused by neuronal dysfunction and not neurodegeneration, which implies that it can be corrected, as we show here in flies by the addition of PtdSer to the food.

Acknowledgments

We thank the Bloomington, Harvard and Kyoto Drosophila stock centers, and the Developmental Studies Hybridoma bank as well as Bart De Strooper, Patrick Callaerts, Sha Liu, Edwin S. Levitan, Wim Vandenberghe and Rose Goodchild for reagents. We thank Bart De Strooper, Sha Liu, Wim Vandenberghe, Georg Halder, Vanessa A. Morais, Rose Goodchild, Joseph McInnes, Sabine Kuenen, António Laranjeira, Elsa Lauwers, Ana Rita Santos, the VIB BioImaging core facility and all members of the Verstreken lab for discussions and help.

This work was supported by an ERC Consolidator Grant, the FWO Vlaanderen, the Hercules Foundation, IWT, BELSPO-IAP, a Methusalem grant of the Flemish government, Opening the Future, the Vlaamse Parkinsonliga and VIB. J.S.V. is supported by the Fundação para a Ciência e a Tecnologia (FCT), D.V. is supported by the FWO and P.V. is a member of the FENS Kavli Network of Excellence.

Author contributions:

J.S.V., G.E., D.V., K.M., L.D. and S.R. performed research and/or analyzed the data. J.S.V., G.E., K.M. and P.V. designed experiments. P.S. and C.K. provided iPSC. J.S.V. and P.V. made the Figures, wrote the paper and conceptualized the study. All authors discussed the results and commented on the manuscript.

Declaration of Interests

The authors declare no conflicts of interest.

References

- Ahmed, R.M., Newcombe, R.E.A., Piper, A.J., Lewis, S.J., Yee, B.J., Kiernan, M.C., and Grunstein, R.R. (2016). Sleep disorders and respiratory function in amyotrophic lateral sclerosis. *Sleep Med. Rev.* 26, 33–42.
- Area-Gomez, E. (2014). Assessing the function of mitochondria-associated ER membranes. *Methods Enzymol.* 547, 181–197.
- Arvan, P., and Castle, D. (1998). Sorting and storage during secretory granule biogenesis: looking backward and looking forward. *Biochem. J.* 332, 593–610.
- Braak, H., Del Tredici, K., Rüb, U., De Vos, R.A.I., Jansen Steur, E.N.H., and Braak, E. (2003). Staging of brain pathology related to sporadic Parkinson's disease. *Neurobiol. Aging* 24, 197–211.
- de Brito, O.M., and Scorrano, L. (2008). Mitofusin 2 tethers endoplasmic reticulum to mitochondria. *Nature* 456, 605–610.
- Brogiolo, W., Stocker, H., Ikeya, T., Rintelen, F., Fernandez, R., and Hafen, E. (2001). An evolutionarily conserved function of the drosophila insulin receptor and insulin-like peptides in growth control. *Curr. Biol.* 11, 213–221.
- Burman, J.L., Yu, S., Poole, A.C., Decal, R.B., and Pallanck, L. (2012). Analysis of neural subtypes reveals selective mitochondrial dysfunction in dopaminergic neurons from parkin mutants. *Proc. Natl. Acad. Sci.* 109, 10438–10443.
- Carvalho, M., Sampaio, J.L., Palm, W., Brankatschk, M., Eaton, S., and Shevchenko, A. (2012). Effects of diet and development on the *Drosophila* lipidome. *Mol. Syst. Biol.* 8, 1–17.
- Celardo, I., Costa, A.C., Lehmann, S., Jones, C., Wood, N., Mencacci, N.E., Mallucci, G.R., Loh, S.H.Y., and Martins, L.M. (2016). Mitofusin-mediated ER stress triggers neurodegeneration in

pink1/parkin models of Parkinson's disease. *Cell Death Dis.* 7, e2271.

Chiu, J.C., Low, K.H., Pike, D.H., Yildirim, E., and Edery, I. (2010). Assaying locomotor activity to study circadian rhythms and sleep parameters in *Drosophila*. *J. Vis. Exp.* 43, e2157.

Clark, I.E., Dodson, M.W., Jiang, C., Cao, J.H., Huh, J.R., Seol, J.H., Yoo, S.J., Hay, B.A., and Guo, M. (2006). *Drosophila pink1* is required for mitochondrial function and interacts genetically with parkin. *Nature* 441, 1162–1166.

De Cock, V.C., Vidailhet, M., and Arnulf, I. (2008). Sleep disturbances in patients with parkinsonism. *Nat. Clin. Pract.* 4, 254–266.

Crocker, A., Shahidullah, M., Levitan, I.B., and Sehgal, A. (2010). Identification of a Neural Circuit that Underlies the Effects of Octopamine on Sleep:Wake Behavior. *Neuron* 65, 670–681.

Damiano, M., Gautier, C.A., Bulteau, A.L., Ferrando-Miguel, R., Gouarne, C., Paoli, M.G., Pruss, R., Auchère, F., L'Hermitte-Stead, C., Bouillaud, F., et al. (2014). Tissue- and cell-specific mitochondrial defect in Parkin-deficient mice. *PLoS One* 9, e99898.

Dawson, T.M., and Dawson, V.L. (2010). The role of Parkin in familial and sporadic Parkinson's Disease. *Mov. Disord.* 25, S32-9.

Deerinck, T.J., Bushong, E.A., Thor, A., and Ellisman, M.H. (2010). Ncmir Methods for 3D Em : a new protocol for preparation of biological specimens for serial block face scanning electron microscopy. *Microscopy* 6–8.

Depner, H., Lützkendorf, J., Babkir, H.A., Sigrist, S.J., and Holt, M.G. (2014). Differential centrifugation–based biochemical fractionation of the *Drosophila* adult CNS. *Nat. Protoc.* 9, 2796–2808.

Erpapazoglou, Z., and Corti, O. (2015). The endoplasmic reticulum/mitochondria interface: a

subcellular platform for the orchestration of the functions of the PINK1-Parkin pathway? *Biochem. Soc. Trans.* *43*, 297–301.

Esposito, G., Vos, M., Vilain, S., Swerts, J., Valadas, J.S., Van Meensel, S., Schaap, O., and Verstreken, P. (2013). Aconitase Causes Iron Toxicity in *Drosophila pink1* Mutants. *Plos Genet.* *9*, e1003478.

Fifel, K., Piggins, H., and Deboer, T. (2016). Modeling sleep alterations in Parkinson's disease: How close are we to valid translational animal models? *Sleep Med. Rev.* *25*, 95–111.

Gautier, C.A., Kitada, T., and Shen, J. (2008). Loss of PINK1 causes mitochondrial functional defects and increased sensitivity to oxidative stress. *Proc. Natl. Acad. Sci. U. S. A.* *105*, 11364–11369.

Gautier, C.A., Erpapazoglou, Z., Mouton-Liger, F., Muriel, M.P., Cormier, F., Bigou, S., Duffaure, S., Girard, M., Foret, B., Iannielli, A., et al. (2016). The endoplasmic reticulum-mitochondria interface is perturbed in PARK2 knockout mice and patients with PARK2 mutations. *Hum. Mol. Genet.* *25*, 2972–2984.

Geisler, S., Holmström, K.M., Skujat, D., Fiesel, F.C., Rothfuss, O.C., Kahle, P.J., and Springer, W. (2010). PINK1/Parkin-mediated mitophagy is dependent on VDAC1 and p62/SQSTM1. *Nat. Cell Biol.* *12*, 119–131.

Graham, B.H., Li, Z., Alesii, E.P., Verstecken, P., Lee, C., Wang, J., and Craigen, W.J. (2010). Neurologic dysfunction and male infertility in *Drosophila* porin mutants: a new model for mitochondrial dysfunction and disease. *J Biol Chem.* *285*, 11143–11153.

Greene, J.C., Whitworth, A.J., Kuo, I., Andrews, L.A., Feany, M.B., and Pallanck, L.J. (2003). Mitochondrial pathology and apoptotic muscle degeneration in *Drosophila parkin* mutants. *Proc Natl Acad Sci U S A* *100*, 4078–4083.

Helfrich-Förster, C., and Homberg, U. (1993). Pigment-dispersing hormone-immunoreactive neurons

in the nervous system of wild-type *Drosophila melanogaster* and of several mutants with altered circadian rhythmicity. *J. Comp. Neurol.* *337*, 177–190.

Helle, S.C.J., Kanfer, G., Kolar, K., Lang, A., Michel, A.H., and Kornmann, B. (2013). Organization and function of membrane contact sites. *Biochim. Biophys. Acta - Mol. Cell Res.* *1833*, 2526–2541.

Hendricks, J.C., and Sehgal, A. (2004). Why a fly? Using *Drosophila* to understand the genetics of circadian rhythms and sleep. *Sleep* *27*, 334–342.

Hendricks, J.C., Finn, S.M., Panckeri, K.A., Chavkin, J., Williams, J.A., Sehgal, A., and Pack, A.I. (2000). Rest in *Drosophila* Is a Sleep-like State. *Neuron* *25*, 129–138.

Kasten, M., Kertelge, L., Brüggemann, N., van der Vegt, J., Schmidt, A., Tadic, V., Buhmann, C., Steinlechner, S., Behrens, M.I., Ramirez, A., et al. (2010). Nonmotor Symptoms in Genetic Parkinson Disease. *Arch. Neurol.* *67*, 670–676.

Kim, H., Huang, B.X., and Spector, A.A. (2014). Phosphatidylserine in the Brain: Metabolism and Function. *Prog. Lipid Res.* *56*, 1–18.

Koh, K., Evans, J.M., Hendricks, J.C., and Sehgal, A. (2006). A *Drosophila* model for age-associated changes in sleep:wake cycles. *Proc. Natl. Acad. Sci.* *103*, 13843–13847.

Kornmann, B., Currie, E., Collins, S.R., Schuldiner, M., Nunnari, J., Weissman, J.S., and Walter, P. (2009). An ER-mitochondria tethering complex revealed by a synthetic biology screen. *Science* *325*, 477–481.

Kremer, A., Lippens, S., Bartunkova, S., Asselbergh, B., Blanpain, C., Fendrych, M., Goossens, A., Holt, M., Janssens, S., Krols, M., et al. (2015). Developing 3D SEM in a broad biological context. *J. Microsc.* *259*, 80–96.

Kremer, J.R., Mastronarde, D.N., and McIntosh, J.R. (1996). Computer visualization of three-

dimensional image data using IMOD. *J. Struct. Biol.* *116*, 71–76.

Krols, M., van Isterdael, G., Asselbergh, B., Kremer, A., Lippens, S., Timmerman, V., and Janssens, S. (2016). Mitochondria-associated membranes as hubs for neurodegeneration. *Acta Neuropathol.* *131*, 505–523.

Kula-Eversole, E., Nagoshi, E., Shang, Y., Rodriguez, J., Allada, R., and Rosbash, M. (2010). Surprising gene expression patterns within and between PDF-containing circadian neurons in *Drosophila*. *Proc. Natl. Acad. Sci. U. S. A.* *107*, 13497–13502.

Kunst, M., Tso, M.C.F., Ghosh, D.D., Herzog, E.D., and Nitabach, M.N. (2015). Rhythmic control of activity and sleep by class B1 GPCRs. *Crit. Rev. Biochem. Mol. Biol.* *50*, 18–30.

Lee, H.M., and Koh, S. (2015). Many Faces of Parkinson's Disease: Non-Motor Symptoms of Parkinson's Disease. *J. Mov. Disord.* *8*, 92–97.

Lill, C., and Klein, C. (2015). The Neurogenetics of Parkinson's disease and Putative Links to Other Neurodegenerative Disorders. In *Parkinson's Disease: Molecular Mechanisms Underlying Pathology*, P. Verstreken, ed. pp. 1–49.

Loh, Y.P. (1987). Peptide Precursor Processing Enzymes within Secretory Vesicles. *Ann. N. Y. Acad. Sci.* *493*, 292–307.

Merkle, F.T., Maroof, A., Wataya, T., Sasai, Y., Studer, L., Eggan, K., and Schier, A.F. (2015). Generation of neuropeptidergic hypothalamic neurons from human pluripotent stem cells. *Development* *142*, 633–643.

Miskiewicz, K., Schürmann, F.W., and Pyza, E. (2008). Circadian release of pigment-dispersing factor in the visual system of the Housefly, *Musca domestica*. *J. Comp. Neurol.* *509*, 422–435.

Miskiewicz, K., Jose, L.E., Yeshaw, W.M., Valadas, J.S., Swerts, J., Munck, S., Feiguin, F., Dermaut,

B., and Verstreken, P. (2014). HDAC6 is a bruchpilot deacetylase that facilitates neurotransmitter release. *Cell Rep.* 8, 94–102.

Morais, V.A., Verstreken, P., Roethig, A., Smet, J., Snellinx, A., Vanbrabant, M., Haddad, D., Frezza, C., Mandemakers, W., Vogt-Weisenhorn, D., et al. (2009). Parkinson's disease mutations in PINK1 result in decreased Complex I activity and deficient synaptic function. *EMBO Mol. Med.* 1, 99–111.

Morton, A.J. (2013). Circadian and sleep disorder in Huntington's disease. *Exp. Neurol.* 243, 34–44.

Munhoz, R.P., Moro, A., Silveira-Moriyama, L., and Teive, H.A. (2015). Non-motor signs in Parkinson's disease: a review. *Arq. Neuropsiquiatr.* 73, 454–462.

De Pablo-Fernández, E., Breen, D.P., Bouloux, P.M., Barker, R.A., Foltynie, T., and Warner, T.T. (2017). Neuroendocrine abnormalities in Parkinson's disease. *J. Neurol. Neurosurg. Psychiatry* 88, 176–185.

Paillusson, S., Stoica, R., Gomez-Suaga, P., Lau, D.H.W., Mueller, S., Miller, T., and Miller, C.C.J. (2016). There's Something Wrong with my MAM; the ER-Mitochondria Axis and Neurodegenerative Diseases. *Trends Neurosci.* 39, 146–157.

Park, J., Lee, S.B., Lee, S., Kim, Y., Song, S., Kim, S., Bae, E., Kim, J., Shong, M., Kim, J.-M., et al. (2006). Mitochondrial dysfunction in *Drosophila* PINK1 mutants is complemented by parkin. *Nature* 441, 1157–1161.

Park, J., Lee, G., and Chung, J. (2009). The PINK1-Parkin pathway is involved in the regulation of mitochondrial remodeling process. *Biochem. Biophys. Res. Commun.* 378, 518–523.

Peeraully, T., Yong, M.H., Chokroverty, S., and Tan, E.K. (2012). Sleep and Parkinson's disease: A review of case-control polysomnography studies. *Mov. Disord.* 27, 1729–1737.

Pesah, Y., Pham, T., Burgess, H., Middlebrooks, B., Verstreken, P., Zhou, Y., Harding, M., Bellen, H.,

and Mardon, G. (2004). *Drosophila parkin* mutants have decreased mass and cell size and increased sensitivity to oxygen radical stress. *Development* 131, 2183–2194.

Peter-Derex, L., Yammine, P., Bastuji, H., and Croisile, B. (2015). Sleep and Alzheimer's disease. *Sleep Med. Rev.* 19, 29–38.

Pickrell, A.M., and Youle, R.J. (2015). The roles of PINK1, Parkin, and mitochondrial fidelity in parkinson's disease. *Neuron* 85, 257–273.

Politis, M., Wu, K., Molloy, S., Bain, P.G., Chaudhuri, K.R., and Piccini, P. (2010). Parkinson's disease symptoms: The patient's perspective. *Mov. Disord.* 25, 1646–1651.

Poole, A.C., Thomas, R.E., Yu, S., Vincow, E.S., and Pallanck, L. (2010). The mitochondrial fusion-promoting factor mitofusin is a substrate of the PINK1/parkin pathway. *PLoS One* 5, e10054.

Poston, C.N., Krishnan, S.C., and Bazemore-Walker, C.R. (2013). In-depth proteomic analysis of mammalian mitochondria-associated membranes (MAM). *J. Proteomics* 79, 219–230.

Prudent, J., Zunino, R., Sugiura, A., Mattie, S., Shore, G.C., and McBride, H.M. (2015). MAPL SUMOylation of Drp1 Stabilizes an ER/Mitochondrial Platform Required for Cell Death. *Mol. Cell* 59, 941–955.

Rao, S., Lang, C., Levitan, E.S., and Deitcher, D.L. (2001). Visualization of Neuropeptide Expression, Transport, and Exocytosis in *Drosophila melanogaster*. *J. Neurobiol.* 49, 159–172.

Renn, S.C., Park, J.H., Rosbash, M., Hall, J.C., and Taghert, P.H. (1999). A pdf Neuropeptide Gene Mutation and Ablation of PDF Neurons Each Cause Severe Abnormalities of Behavioral Circadian Rhythms in *Drosophila*. *Cell* 99, 791–802.

Richter, C., Woods, I.G., and Schier, A.F. (2014). Neuropeptidergic Control of Sleep and Wakefulness. *Annu. Rev. Neurosci.* 37, 503–531.

Rijk, M.C. de, Tzourio, C., Breteler, M.M.B., Dartigues, J.F., Amaducci, L., Lopez-Pousa, S., Manubens-Bertran, J.M., Alperovitch, A., Rocca, W.A., and EUROPARKINSON Study Group (1997). Prevalence of parkinsonism and Parkinson's disease in Europe: the EUROPARKINSON collaborative study. *J. Neurol. Neurosurg. Psychiatry* 62, 10–15.

Rulifson, E.J., Kim, S.K., and Nusse, R. (2002). Ablation of Insulin-Producing Neurons in Flies : Growth and Diabetic Phenotypes. *Science* 296, 1118–1120.

Schneider, C.A., Rasband, W.S., and Eliceiri, K.W. (2012). NIH Image to ImageJ: 25 years of image analysis. *Nat. Methods* 9, 671–675.

Seibler, P., Graziotto, J., Jeong, H., Simunovic, F., Klein, C., and Krainc, D. (2011). Mitochondrial Parkin Recruitment Is Impaired in Neurons Derived from Mutant PINK1 Induced Pluripotent Stem Cells. *J. Neurosci.* 31, 5970–5976.

Shivanandan, A., Radenovic, A., and Sbalzarini, I.F. (2013). MosaicIA: an ImageJ/Fiji plugin for spatial pattern and interaction analysis. *BMC Bioinformatics* 14, 1–10.

Stichel, C.C., Augustin, M., Kühn, K., Zhu, X.R., Engels, P., Ullmer, C., and Lübbert, H. (2000). Parkin expression in the adult mouse brain. *Eur. J. Neurosci.* 12, 4181–4194.

Stoleru, D., Peng, Y., Agosto, J., and Rosbash, M. (2004). Coupled oscillators control morning and evening locomotor behaviour of *Drosophila*. *Nature* 431, 862–868.

Taymans, J.M., Van Den Haute, C., and Baekelandt, V. (2006). Distribution of PINK1 and LRRK2 in rat and mouse brain. *J. Neurochem.* 98, 951–961.

Valadas, J.S., Vos, M., and Verstreken, P. (2015). Therapeutic strategies in Parkinson's disease: What we have learned from animal models. *Ann. N. Y. Acad. Sci.* 1338, 16–37.

Vos, M., Geens, A., Böhm, C., Deaulmerie, L., Swerts, J., Rossi, M., Craessaerts, K., Leites, E.P.,

- Seibler, P., Rakovic, A., et al. (2017). Cardiolipin promotes electron transport between ubiquinone and complex I to rescue PINK1 deficiency. *J. Cell Biol.* *216*, 1–14.
- Vosko, A.M., Schroeder, A., Loh, D.H., and Colwell, C.S. (2007). Vasoactive intestinal peptide and the mammalian circadian system. *Gen. Comp. Endocrinol.* *152*, 165–175.
- Wang, L., Meece, K., Williams, D.J., Lo, K.A., Zimmer, M., Heinrich, G., Carli, J.M., Leduc, C.A., Sun, L., Zeltser, L.M., et al. (2014). Differentiation of hypothalamic-like neurons from human pluripotent stem cells. *J. Clin. Invest.* *1*, 1–13.
- Wang, X., Winter, D., Ashrafi, G., Schlehe, J., Wong, Y.L., Selkoe, D., Rice, S., Steen, J., Lavoie, M.J., and Schwarz, T.L. (2011). PINK1 and Parkin target miro for phosphorylation and degradation to arrest mitochondrial motility. *Cell* *147*, 893–906.
- Westhead, E.W. (1987). Lipid Composition and Orientation in Secretory Vesicles. *Ann. N. Y. Acad. Sci.* *493*, 92–100.
- Wong, M.Y., Zhou, C., Shakiryanova, D., Lloyd, T.E., Deitcher, D.L., and Levitan, E.S. (2012). Neuropeptide delivery to synapses by long-range vesicle circulation and sporadic capture. *Cell* *148*, 1029–1038.
- Zanon, A., Kalvakuri, S., Rakovic, A., Foco, L., Guida, M., Schwienbacher, C., Serafin, A., Rudolph, F., Trilck, M., Grünewald, A., et al. (2017). SLP-2 interacts with Parkin in mitochondria and prevents mitochondrial dysfunction in Parkin-deficient human iPSC-derived neurons and *Drosophila*. *Hum. Mol. Genet.* *26*, 2412–2425.

Figure titles and legends

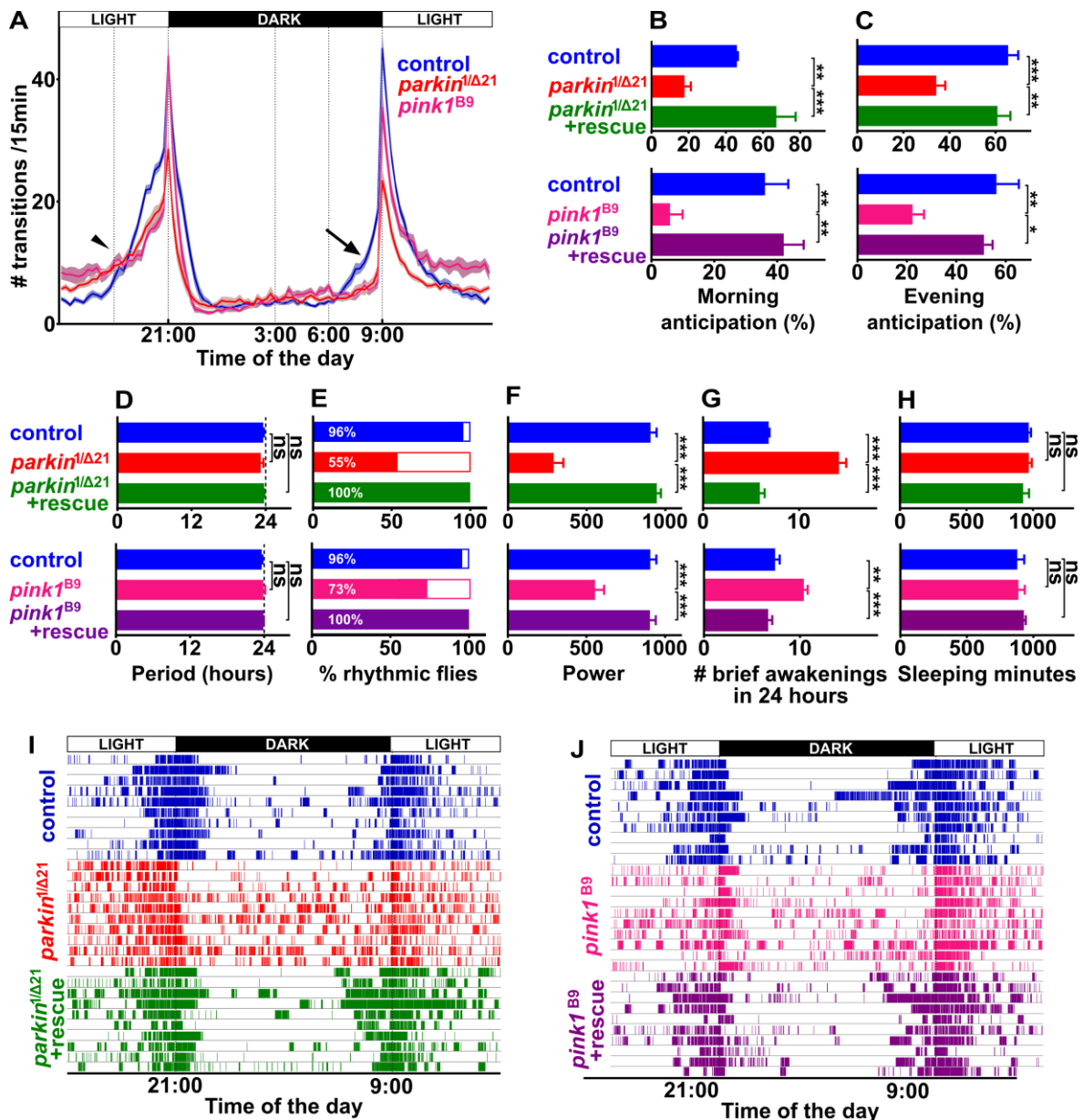


Figure 1. Circadian and sleep pattern defects in *parkin* and *pink1* mutant flies. Related to Figure S1 and Figure S2.

(A-C) 24 h average activity plotted as the number of infrared beam breaks measured per 15 min of control, *parkin* and *pink1* null mutant flies (A) and quantification of morning anticipation (arrow in A) (B) and evening anticipation (arrowhead in A) (C). Defects in *parkin* and *pink1* mutants are rescued by a genomic fragment containing the wild type gene. n=3-22 assays with >25 flies per assay. * $p < 0.05$, ** $p < 0.01$, *** $p < 0.001$ by Bonferroni's test following one-way ANOVA. Data are represented as mean \pm SEM.

(D-F) Quantification of the circadian period (**D**), the percentage of rhythmic flies (**E**) and the power of the circadian cycle (**F**) of controls, *parkin* and *pink1* mutants (without and with a genomic rescue construct) entrained in a 12 h light-12 h dark cycle and tested in constant dark conditions. In D and F only rhythmic flies were quantified. n=20-23 flies. ns: not significant, *** $p < 0.001$ by Bonferroni's test following one-way ANOVA. Data are represented as mean \pm SEM.

(G-J) Quantification of the number of brief awakenings in a 24 h period (**G**) and the number of sleeping minutes in a 24 h period (**H**) for control flies, *parkin* and *pink1* mutants (with or without a genomic rescue construct) and 24 h activity plots of individual flies (rows) (I-J). Each vertical bar represents an active minute. n=5-9 assays with more than 25 flies per assay. ns: not significant, ** $p < 0.01$, *** $p < 0.001$, by Bonferroni's test following one-way ANOVA. Data are represented as mean \pm SEM.

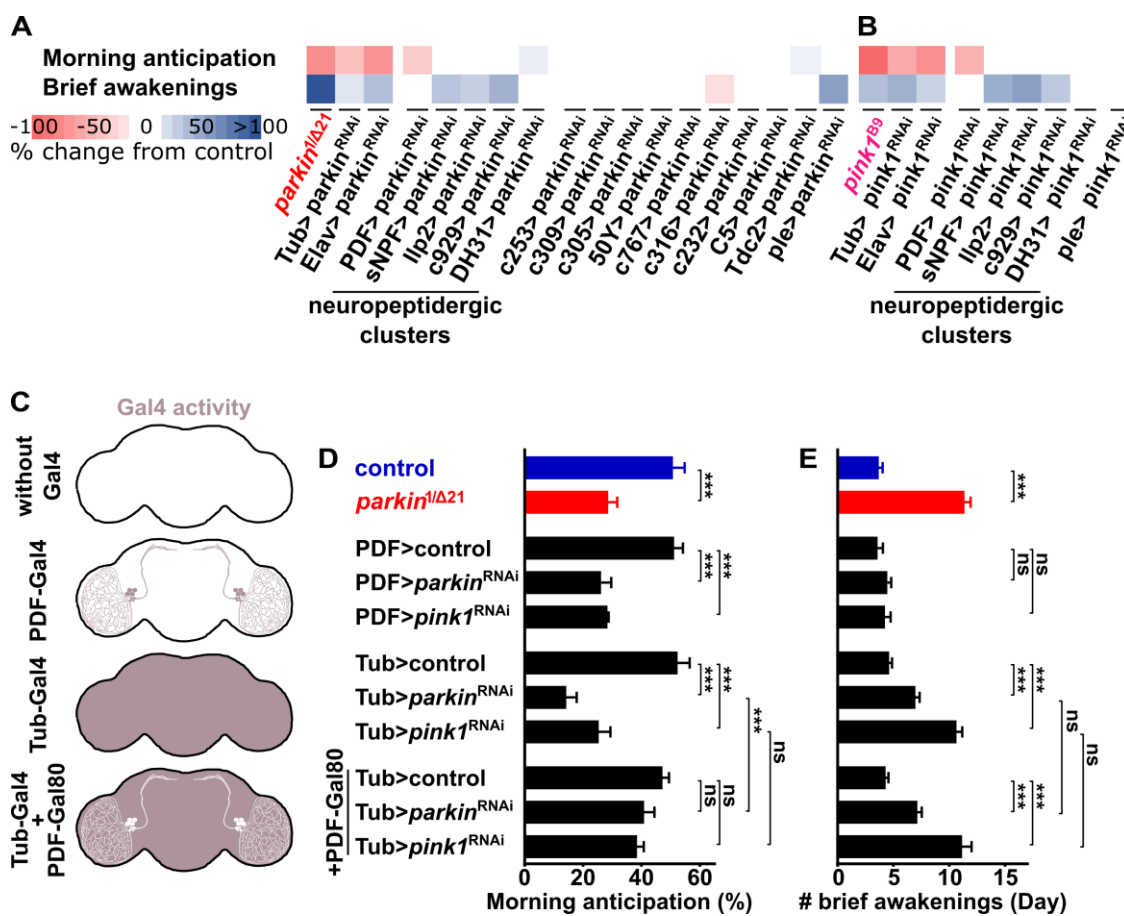


Figure 2. Parkin and Pink1 function in neuropeptidergic neurons to control circadian rhythms and sleep patterns. Related to Figure S2.

(A-B) Schematic representation of a mini-screen where Parkin (**A**) or Pink1 (**B**) were downregulated using RNAi and different (indicated) Gal4 lines. *parkin* and *pink1* null mutants are included for comparison. Shades of blue and red indicate % change from control (increase or decrease respectively) and only significantly different changes are included ($p < 0.05$, Mann-Whitney test). Note that RNAi expression with PDF-Gal4 recapitulates the morning anticipation defect while several other neuronal

drivers, including the Ilp2-Gal4 recapitulate the brief awakening defect (n=3-8 assays with more than 25 flies per assay).

(C) LNV specific requirements for Parkin and Pink1 function to elicit morning anticipation defects. Graphic representation of where Gal4 is present to drive RNAi expression. PDF-Gal4 expresses RNAi only in LNV neurons and Tubulin-Gal4 broadly expresses RNAi. In the presence of Tubulin-Gal4, PDF-Gal80 neutralizes Gal4 activity in LNV neurons, while Gal4 is still active in the remaining neurons.

(D-E) Quantification of morning anticipation **(D)** and brief awakenings **(E)** in flies with Parkin or Pink1 downregulated in the clusters outlined in (C). Note that Pink1 and Parkin function in LNVs alone is sufficient to drive morning anticipation. n=14-32 flies. ns: not significant, *** $p < 0.001$ by Bonferroni's test following one-way ANOVA. Data are represented as mean \pm SEM.

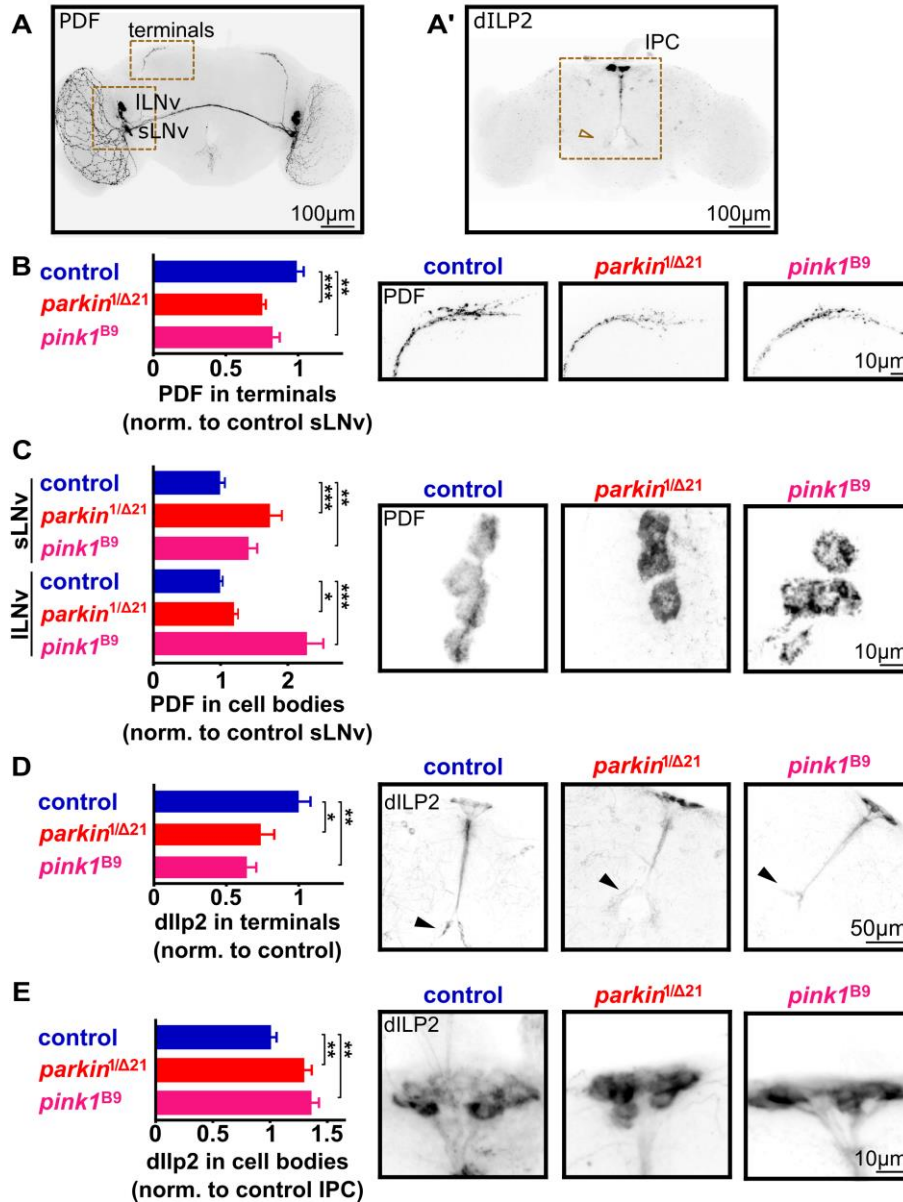


Figure 3. Neuropeptides accumulate in the cell bodies of *parkin* and *pink1* mutant neurons. Related to Figure S3.

(A-A') *Drosophila* brains labeled with anti-PDF (A) or anti-dILP2 (A'). The neuronal cell body is indicated, as are the locations of terminals (arrowhead in A'). The orange boxed areas indicate the regions that are shown in subsequent panels and figures.

(B-E) Quantification of labeling intensity and images of anti-PDF labeled LNv terminals (B) and cell bodies (C), dILP2 labeled neurons (D) and cell bodies (E). Animals were dissected at *Zeitgeber* time 23. n=37-47 animals in B and C; 25-69 animals in D and E. * $p < 0.05$, ** $p < 0.01$, *** $p < 0.001$ by Bonferroni's test following one-way ANOVA. Data are represented as mean \pm SEM.

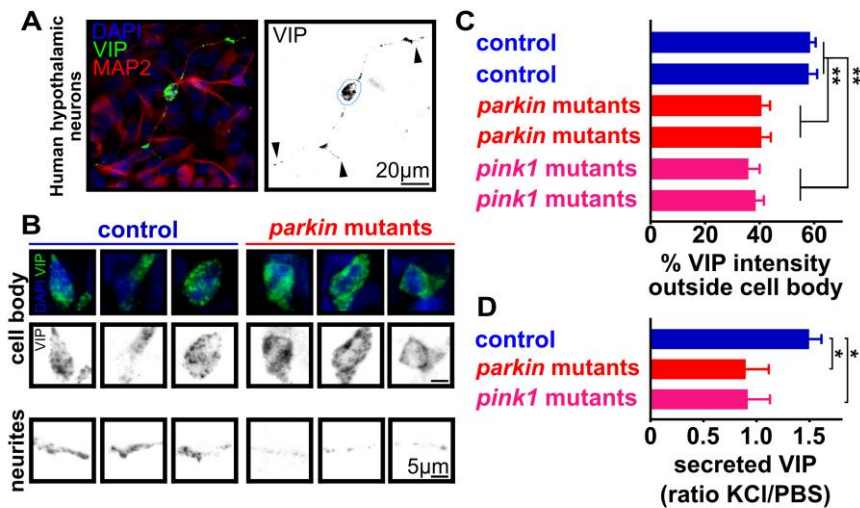


Figure 4. *parkin* and *pink1* mutant human hypothalamic neurons release less VIP. Related to Figure S4.

(A) Images of human hypothalamic neurons from induced pluripotent stem cells (iPSC) of non-diseased people (control) labelled with DAPI (nucleus), anti-VIP and anti-MAP2 showing VIP in the cell body (dashed circle) and in the neurites (arrows).

(B-C) Images of cell bodies and neurites of control and *parkin* mutant human hypothalamic neurons labelled with anti-VIP and DAPI (3 representative examples) (B) and quantification of anti-VIP labelling intensity outside cell bodies in neurons of 2 independent controls and 4 independent Parkinson's disease patients with *parkin* or *pink1* mutations indicating lower VIP levels in neurites of mutant cells (C). n=22-74 cells per condition from 2 independent differentiations for all cell lines. ** $p < 0.01$ by Bonferroni's test following one-way ANOVA. Data are represented as mean \pm SEM.

(D) Quantification of VIP release into the medium measured by ELISA when neuronal cultures are chemically stimulated with 60mM KCl. Data for control, *parkin* and *pink1* mutant human neurons are pooled (n=4-6 assays per condition) and normalized to measurements in non-stimulated conditions. * $p < 0.05$ by Bonferroni's test following one-way ANOVA. Data are represented as mean \pm SEM.

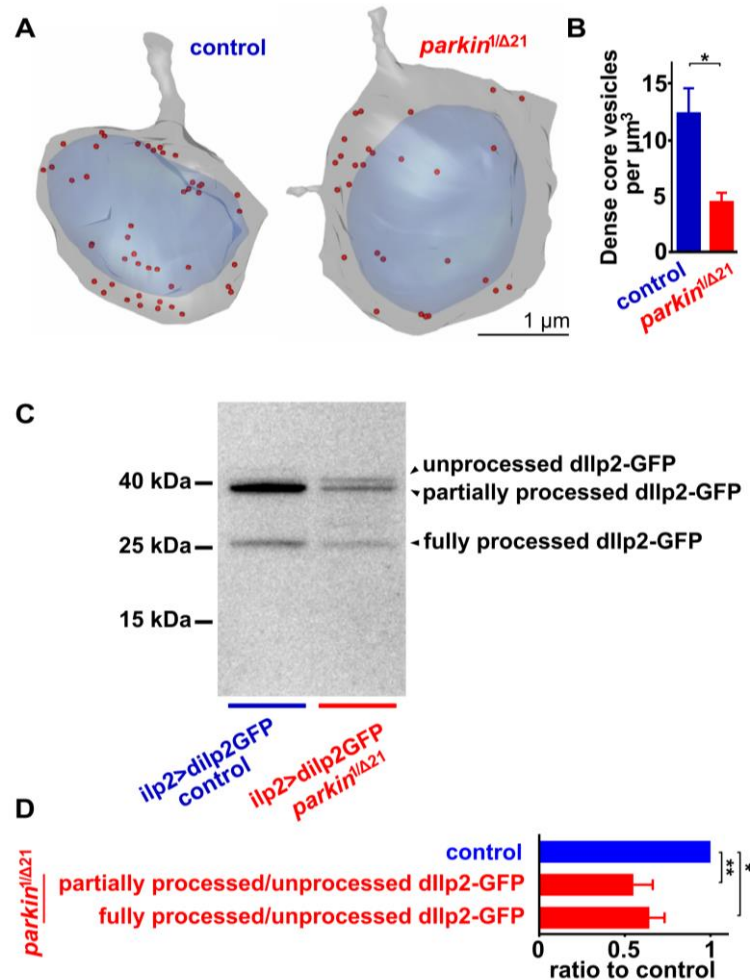


Figure 5. Dense core vesicle number and neuropeptide processing are decreased in LNv of *parkin* mutants. Related to Figure S5.

(**A-B**) 3D-reconstructions of PDF-HRP-labeled LNv cell bodies using focused ion beam scanning electron microscopy (FIB-SEM) stacks, indicating the nucleus (blue), the cytoplasm (grey) and DCVs (red) in control fly and a *parkin* mutant fly (**A**) and quantification of the number of DCVs per cellular volume (**B**). For all quantifications, we ensured the nucleus and the large majority of the cell body was present in our reconstructions. $n=6-7$ reconstructions from 4 control and 4 *parkin* mutant brains. $*p<0.05$, by Mann-Whitney test.

(**C-D**) Western blot of adult fly heads expressing dllp2-GFP in IPC under control of Ilp2-Gal4 in control and *parkin* mutant flies probed with anti-GFP. The bands for unprocessed, partially processed and fully processed dllp2-GFP are indicated (**C**) and the quantification of the intensity of each band normalized to the unprocessed neuropeptide (**D**). $n=4$ independent experiments. $*p<0.05$, $**p<0.01$ by Bonferroni's test following one-way ANOVA. Data are represented as mean \pm SEM.

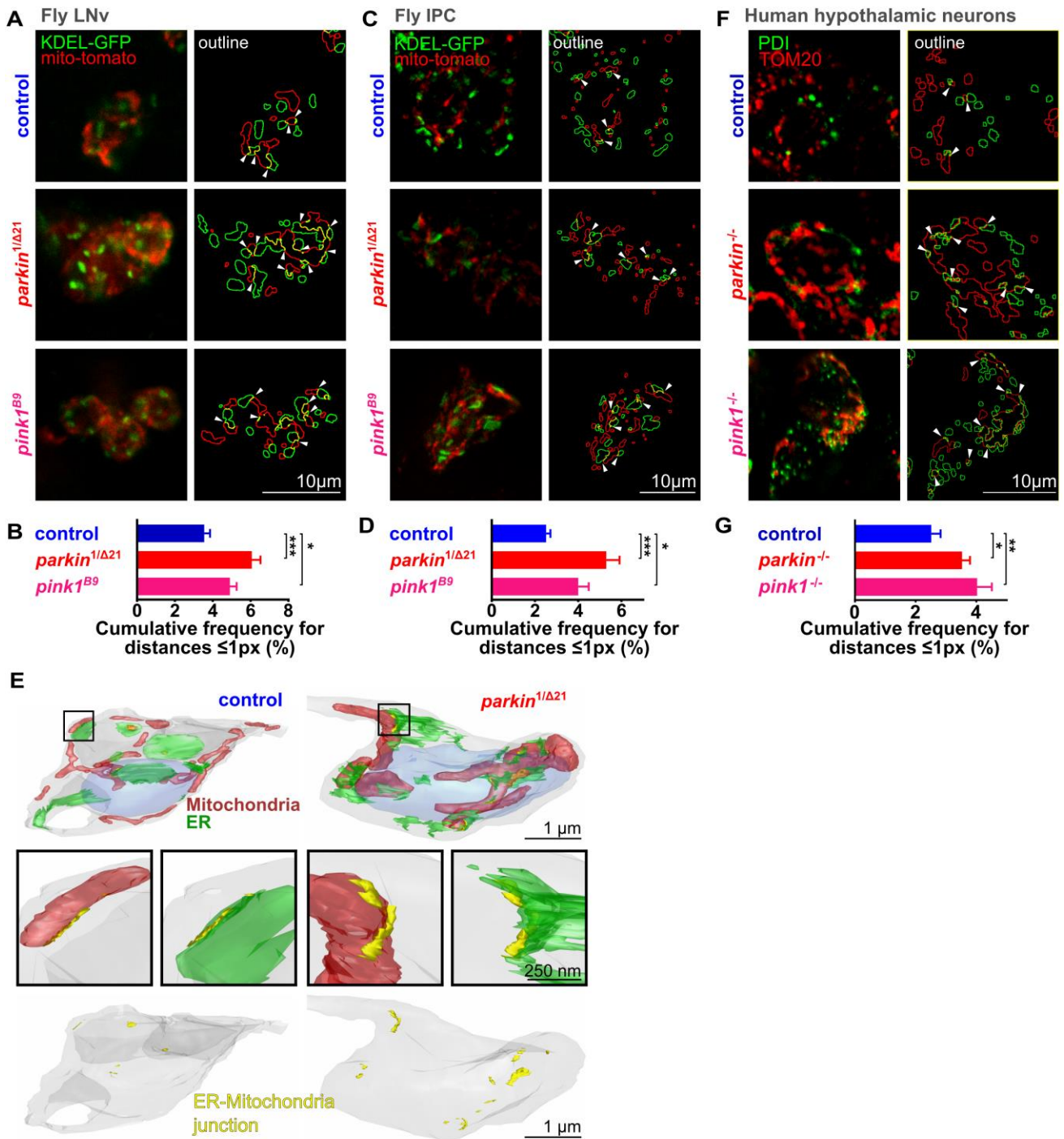


Figure 6. ER-mitochondria contacts are increased in *parkin* and *pink1* mutant neuropeptidergic neurons. Related to Figure S6.

(A-D) Images of LNV neuron cell bodies (A) and IPC neuron cell bodies (C) that express KDEL-GFP (ER, green) and mito-tdTomato (mitochondria, red) of controls, *parkin* and *pink1* mutants (A, C, left), and the outline of ER and mitochondria labeling where arrowheads indicate where the labeling connects (A, C, right). Quantification of the extent of the contacts between ER and mitochondria in LNV (B) and IPC (D) cell bodies of *parkin* and *pink1* mutants (e.g. quantification of the frequency of ER pixels within a distance of one pixel from mitochondria). n=7-9 brains for B and 16-24 brains for

C per condition. * $p < 0.05$, *** $p < 0.001$ by Bonferroni's test following one-way ANOVA. Data are represented as mean \pm SEM.

(E) 3D model of an LNv neuron cell body generated from a FIB-SEM data stack of a control and a *parkin* mutant fly indicating ER (green), mitochondria (red) and the contacts between them (locations where the organelles are < 30 nm apart, yellow). Nucleus: blue, cytoplasm: grey, box: inset.

(F-G) Images of induced hypothalamic neurons of controls, *parkin* and *pink1* mutant patients (F, left) labelled with anti-PDI (ER, green) and anti-TOM20 (mitochondria, red) and the outline of ER and mitochondria labeling where arrowheads indicate where the labeling connects (F, right). Quantification of the extent of the contacts between ER and mitochondria in control, *parkin* and *pink1* mutant hypothalamic differentiated neurons. $n = 16-20$ neurons per genotype from two independent differentiations. * $p < 0.05$, ** $p < 0.01$ by Bonferroni's test following one-way ANOVA. Data are represented as mean \pm SEM.

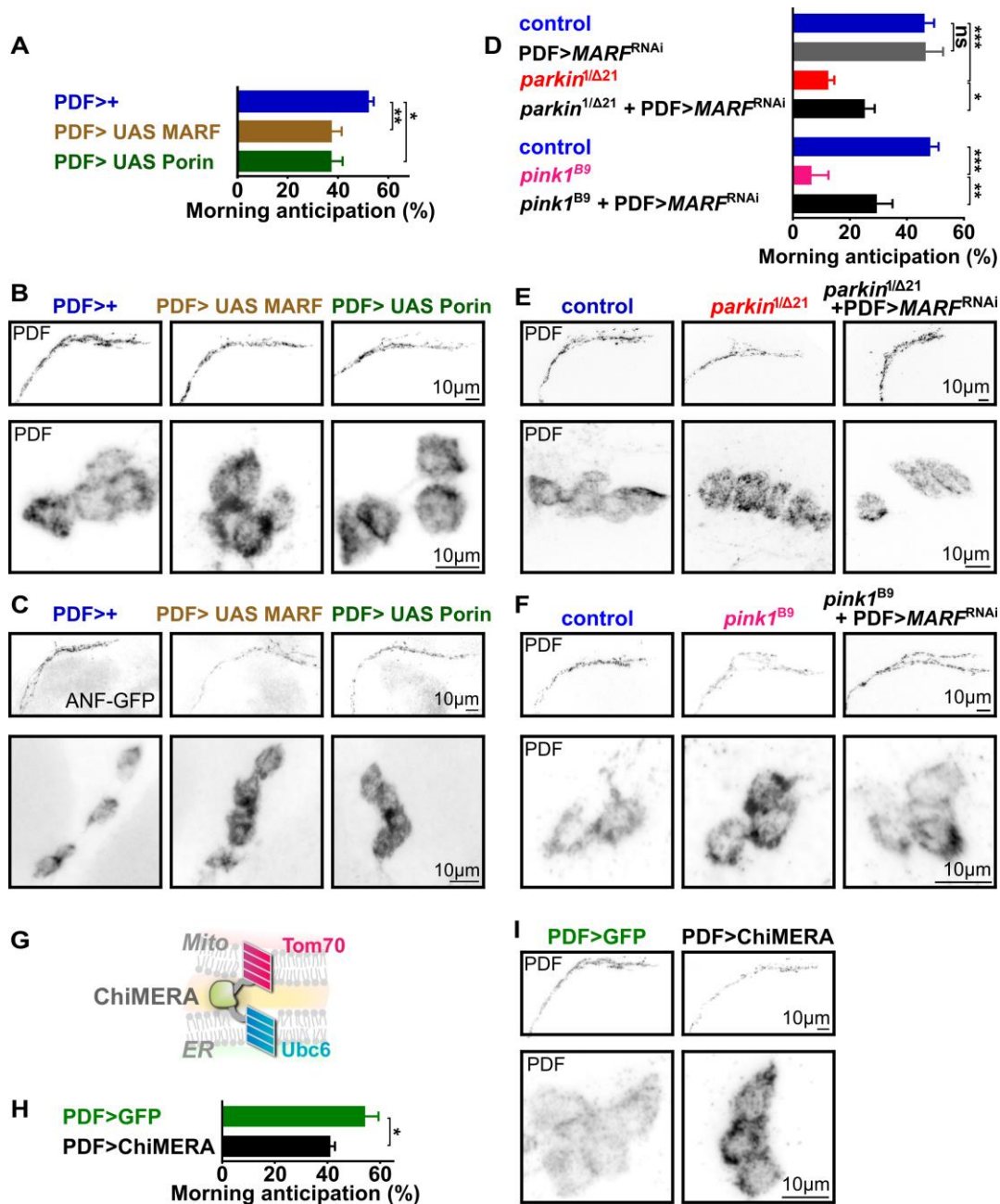


Figure 7. Increased ER-mitochondria contacts in *parkin* and *pink1* mutants are causal to morning anticipation defects. Related to Figure S7.

(A) Quantification of morning anticipation upon overexpression of MARF or Porin in LNV (PDF-Gal4). n=4-6 assays with 25 flies each. * $p < 0.05$, ** $p < 0.01$ by Bonferroni's test following one-way ANOVA. Data are represented as mean \pm SEM.

(B-C) Images of LNV neuronal terminals and cell bodies of animals overexpressing MARF or Porin in LNV (PDF-Gal4) and labeled with anti-PDF (B), or also expressing ANF-GFP, where GFP was imaged (C). Note the increased neuropeptide labeling in the cell bodies and reduced labeling at terminals. Quantification in Figure S7A-D.

(D) Quantification of morning anticipation upon downregulation of *MARF* in LNV (PDF-Gal4) of *parkin* and *pink1* mutants. Note that this rescues the defects of *parkin* and *pink1* mutants. n=4-6 assays with 25 flies each. ns: not significant; * $p < 0.05$, ** $p < 0.01$, *** $p < 0.001$ by Bonferroni's test following one-way ANOVA. Data are represented as mean \pm SEM.

(E-F) Images of LNV neuronal terminals and cell bodies upon downregulation of *MARF* in LNV (PDF-Gal4) of *parkin* (E) and *pink1* (F) mutants, labeled with anti-PDF. Note that this rescues the defects of *parkin* and *pink1* mutants. Quantification in Figure S7E-H.

(G) ChiMERA bridges the mitochondrial and ER membrane to induce additional contacts between these organelles.

(H) Quantification of morning anticipation upon ChiMERA overexpression in LNV (PDF-Gal4). Note this phenocopies *pink1* and *parkin* mutants. n=5-8 assays with 25 flies each. * $p < 0.05$ by Mann-Whitney test. Data are represented as mean \pm SEM.

(I) Images of LNV neuronal terminals and cell bodies upon overexpression of ChiMERA in LNV (PDF-Gal4) labeled with anti-PDF. Note the increased neuropeptide labeling in the cell bodies and reduced labeling at terminals. Quantification in Figure S7M-N.

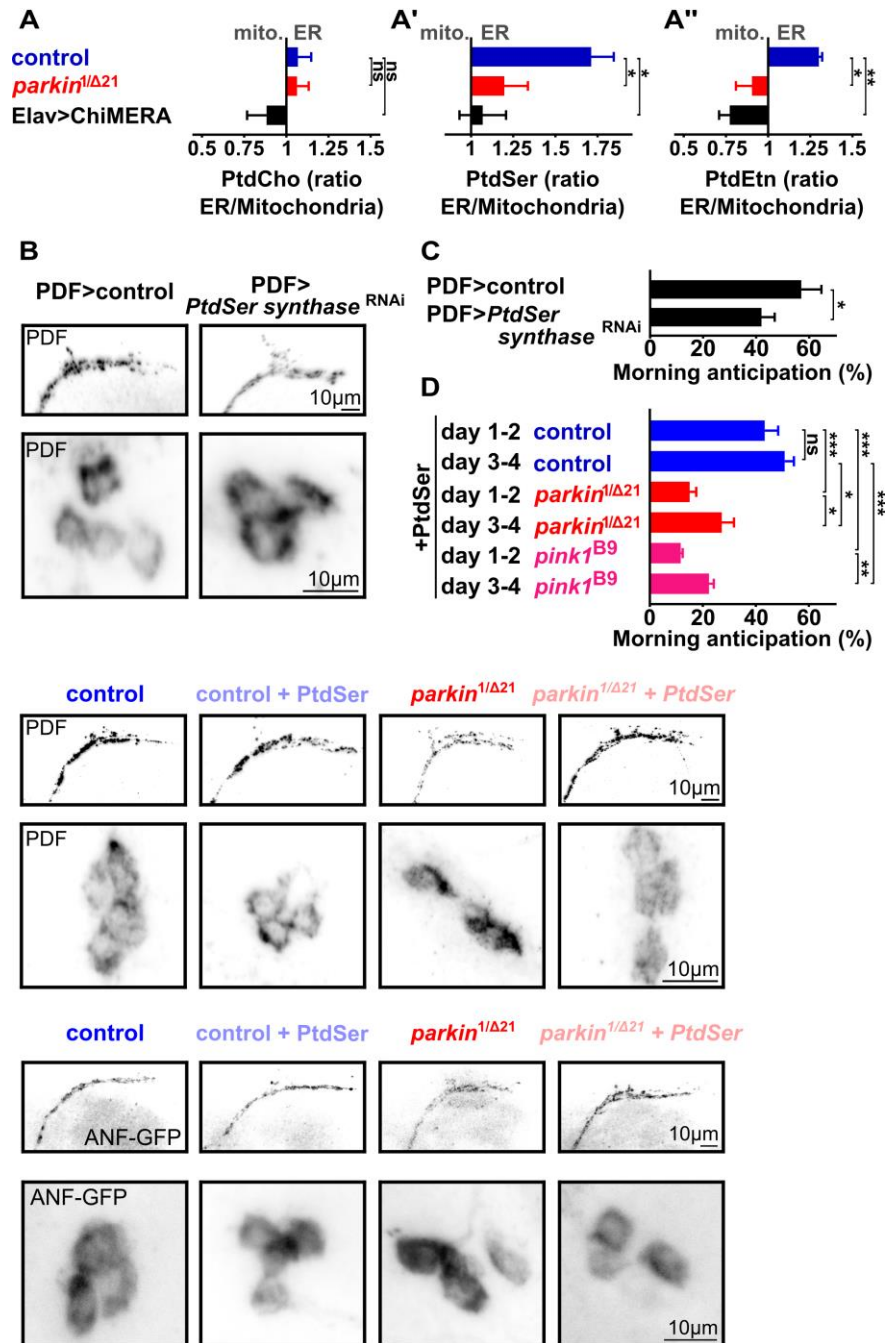


Figure 8. PtdSer depletion from the ER is causative to circadian and sleep pattern defects. Related to Figure S8.

(A) Ratio of the amount of phosphatidylcholine (PtdCho, A), phosphatidylserine (PtdSer, A') and phosphatidylethanolamine (PtdEtn, A'') measured by mass-spectrometry (MS) shotgun lipidomics in the ER fraction to the amount measured in the mitochondrial fraction of heads of control flies, *parkin* mutant flies and flies expressing ChiMERA in neurons (Elav>ChiMERA). A ratio of 1 (indicated by the line) means the concentration of the indicated lipid in ER and mitochondria are identical. A ratio above 1 indicates enrichment in the ER and a ratio below 1 indicates enrichment in the mitochondria.

n=3-5 independent assays (fly collection and MS). ns: not significant, $*p<0.05$ by Bonferroni's test following one-way ANOVA. Data are represented as mean \pm SEM.

(B) Images of LNV neuronal terminals and cell bodies upon expression of RNAi to PtdSer Synthase in LNV (PDF-Gal4) labeled with anti-PDF. Note the increased neuropeptide labeling in the cell bodies and reduced labeling at terminals. Quantification in Figure S8F-G.

(C) Quantification of morning anticipation upon expression of RNAi for PtdSer Synthase in LNV (PDF-Gal4). Note this phenocopies *pink1* and *parkin* mutants. n=4 assays with 25 flies each. $*p<0.05$ by Mann-Whitney test. Data are represented as mean \pm SEM.

(D) Quantification of morning anticipation upon feeding control, *parkin* and *pink1* mutant flies PtdSer 150 μ M (final concentration in the food). Data for the first two days of feeding (day 1-2) were pooled and data for the consecutive two days of feeding (day 3-4) were pooled. Note that after 3-4 days of feeding the morning anticipation defect is partially rescued, as is the defect in brief awakenings (shown in Figure S8H). Longer periods of feeding do not yield stronger rescue of the morning anticipation phenotype (not shown). n=7 assays with 25 flies each. ns: not significant, $*p<0.05$, $**p<0.01$, $***p<0.001$ by Tukey's test following two-way ANOVA.

(E-F) Images of LNV neuronal terminals and cell bodies upon feeding control and *parkin* mutant flies PtdSer 150 μ M (final concentration in the food) for 4 days, labeled with anti-PDF (**E**), or expressing ANF-GFP, where GFP was imaged (**F**). Quantification in Figure S8I-L. Note the rescue of neuropeptide distribution upon PtdSer feeding. Similarly, PtdSer feeding also rescues dIlp2-GFP distribution defects in the IPC (see Figure S8M-N).

STAR Methods

CONTACT FOR REAGENT AND RESOURCE SHARING

Further information and requests for resources and reagents should be directed to the Lead Contact Patrik Verstreken (patrik.verstreken@kuleuven.vib.be)

Human iPSC were used in accordance with an MTA with the University of Lübeck.

EXPERIMENTAL MODEL AND SUBJECT DETAILS

Fly stocks and maintenance

Drosophila melanogaster fly stocks were handled using standard protocols, kept in a 12 h light/dark cycle and fed a standard *Drosophila* diet consisting of cornmeal, agar, yeast, sucrose, and dextrose. All experimental crosses were kept at 25°C. Mutant and transgenic stocks were obtained from the Bloomington *Drosophila* Stock Center (BDSC), Kyoto Stock Center (DGRC), the Vienna *Drosophila* RNAi stock centre (VDRC) or were gifts (see Key Resources Table for details). *parkin*¹, *parkin*^{Δ21}, *parkin*²⁵ are null mutants of *parkin* and *pink1*^{B9} is a null mutant of *pink1*. Rescue flies express a genomic fragment containing *parkin* or *pink1* (Clark et al., 2006; Pesah et al., 2004). Rescue STOP flies express a genomic fragment containing *parkin* but with a premature STOP codon, preventing Parkin expression (Pesah et al., 2004). *w*¹¹¹⁸ was used as control for *parkin* and *pink1* mutants. Flies expressing an RNAi against luciferase (BDSC 31603) were used as control for all TRIP RNAi lines and flies with an empty landing site (VDRC 60100) were used as control for the KK RNAi lines.

The UAS-ChiMERA construct (Kornmann et al., 2009) was generated using standard cloning procedures (using EcoRI and XhoI to integrate the ChiMERA in a pUAS vector). After confirming the sequence of the plasmid, germline transformation was achieved by injection of embryos at BestGene, (USA) using the VK00037 landing site.

iPSC maintenance and differentiation

iPSC from 2 *parkin* patients with gene deletions and point mutations (lines L3048, male; and L5415, female), 2 *PINK1* patients with a premature STOP codon (lines L2124 and L2126, both females) as well as 2 matched controls (lines L4993 and L5991, both females) (Figure S4B) (Seibler et al., 2011; Zanon et al., 2017) were differentiated into hypothalamic neurons according to a protocol described before (Merkle et al., 2015). Briefly, cells were maintained in matrigel coated plates with mTeSR1 (Stem cell technologies) and medium changes were performed every two days. For hypothalamic neurons differentiation, the supplements and media used are described in Figure S4A. After 14 days, cells were trypsinized and replated with maturation medium. At day 30, coverslips with differentiated neurons were placed over cultured rat glia for 10 days and then prepared for immunolabeling or neuropeptide release experiments.

METHOD DETAILS

Fly activity assay

Male flies were selected from each group to be analyzed in the *Drosophila* Activity Monitor (DAM, from Trikinetics) in a 25°C incubator. 2-5 days old male flies are individually introduced in DAM glass tubes (Chiu et al., 2010). After 24h of habituation, fly activity was recorded for at least 3 consecutive days. The number of assays is indicated in the figure legends. Morning anticipation is defined as the ratio between the increase of the transitions in 3 hours that precede the light change (transitions $3 \rightarrow 0$ subtracted the basal activity, transitions $6 \rightarrow 3$) to the transitions on the 6 hours preceding the lights on event (transitions $3 \rightarrow 0$ + transitions $6 \rightarrow 3$). The morning anticipation score of animals that do not increase their activity in the 3 hours before the lights on event is represented as zero, while the score for animals that increase their activity in the last 3 hours of the dark period is a positive value.

$$\text{morning anticipation (\%)} = \frac{\text{transitions}_{3 \rightarrow 0} - \text{transitions}_{6 \rightarrow 3}}{\text{transitions}_{3 \rightarrow 0} + \text{transitions}_{6 \rightarrow 3}} \times 100$$

The evening anticipation score was calculated with the same formula but taking as reference the lights off event. Brief awakenings are periods of a maximum of 5 minutes with less than 4 transitions between 2 sleep events (Koh et al., 2006). Basal motor performance (waking activity) was evaluated by the number of transitions in an active minute (Chiu et al., 2010). For dark/dark experiments, flies were habituated for 7 days in the 12 h light/dark condition before the lights are turned off and activity was recorded for at least 4 days. Quantification of the circadian period, the percentage of rhythmic flies and the power of the circadian cycle are presented (Chiu et al., 2010). Data analysis was performed with a custom-made Microsoft Excel file and FaasX.

***Drosophila* neuropeptide distribution and mitochondria morphology**

One hour before the lights on event (*Zeitgeber* Time 23), fly brains were dissected in cold PBS, fixed in FA 3.7%, washed with PBS (0.05% Triton-X100), blocked with NGS 10% in PBS (0.05% Triton-X100) for 1 h, incubated overnight at 4°C with antibodies for PDF (PDF C7 Hybridoma Bank 1:50) or dIlp2 (gift from Patrick Callaerts, KU Leuven, 1:500), washed with PBS (0.05% Triton-X100), incubated with secondary anti-mouse or anti-rabbit alexa antibodies for 1 h (1:500), washed with PBS (0.05% Triton-X100), and mounted (in Vectashield) on a microscope slide. Confocal stacks of LNv and IPC neurons were acquired with the Nikon A1R confocal microscope through a 20x NA 0.75, 40X NA1.15 or 60X NA1.2 water immersion lens and signal was quantified in ImageJ (Schneider et al., 2012). Images were summed to quantify the total neuropeptide signal in the neuron.

Staining in human differentiated neurons

After 40 days of differentiation, cells were fixed in 4% PFA for 30 minutes, washed with PBS, blocked with 5% NGS in PBS with 0.3% Triton-X100, incubated overnight at 4°C with antibodies for Vasoactive Intestinal Peptide (VIP, Abcam ab8556 1:100), Microtubule-associated protein 2 (MAP2, sigma M1406 1:1000), β tubulin (Biolegend 8020001 1:1000), TOM20 (sc-11415 1:500) or Protein disulfide-isomerase (PDI, Stressgen SPA-891 1:500), washed with PBS, incubated with secondary anti-mouse or anti-rabbit alexa antibodies for 1 h (1:500), washed with PBS, and mounted on a

microscope slide with ProLong® Diamond Antifade Mountant with DAPI (Thermo Fisher). Images were acquired with the Nikon A1R confocal microscope through a 40X NA1.15 or 60X NA1.2 water immersion lens and signal was quantified with ImageJ (Schneider et al., 2012) and the MOSAIC plugin (Shivanandan et al., 2013).

Neuropeptide secretion

Medium from differentiated neurons at day 40 was changed and collected after 20 min (basal release of neuropeptides). Cells were then incubated for 20 mins with Maturation medium (control) or Maturation medium with 60 mM KCl. Medium was again collected and frozen until analysis (Wang et al., 2014). VIP levels were measured with VIP ELISA Kit (Aviva Systems Biology OKEH00406) and results are reported as the ratio between the induced release (with KCl) and the unstimulated release (control).

ER-mitochondria distance in flies

One hour before the lights on event (*Zeitgeber* Time 23), fly brains were dissected in cold PBS, fixed in FA 3.7%, washed 3 times with PBS (0.05% Triton-X100) and mounted (in Vectashield) on a microscope slide. Images were acquired with the Nikon A1R confocal microscope through a 60X NA1.2 water immersion lens and quantified with ImageJ using the MOSAIC plugin (Shivanandan et al., 2013). Briefly, images of ER and mitochondria were thresholded with ImageJ, such that all ER and mitochondria positive pixels are each visible as an area. These areas are transformed into perimeters (removing the inside of the shape). Using the Mosaic plugin for ImageJ, we computed the minimal distance between each pixel of the ER perimeter to the perimeter of the mitochondria. We then calculated the sum of all the frequencies with a distance below 1 pixel (Fig. 5B, D, F) as a measurement of the proximity of ER and mitochondria.

Western blotting

Samples were homogenized in RIPA buffer with protease inhibitors. Protein concentration was determined using the Quick Start™ Bradford Dye Reagent (BioRad) and measured as absorbance at

600 nm in a GloMax Multi Detection Plate Reader (Promega). After denaturation, samples separated by SDS-PAGE, transferred to a nitrocellulose membrane (Miskiewicz et al., 2014) and probed against GFP (Invitrogen A-11122 1:2000), Calreticulin (abcam ab2907 1:1000), ATP synthase (abcam ab147301:1000) or Discs large (DLG, DSHB 4F3 1:1000). The ECL system (Perkin Elmer) was used for detection and chemiluminescence was imaged using LAS-3000 (Fuji Film). The intensity of bands was quantified with ImageJ (Schneider et al., 2012).

Electron microscopy

Dissected fly brains were fixed in 2% formaldehyde + 2% glutaraldehyde, embedded in agarose and sectioned in 70 μ m thick slices. After permeabilization (PBS Triton-X 100 0.02%), inhibition of endogenous Peroxidase (BLOXALL) and blocking (PBS Triton 0.02%, BSA 0.25%, NGS 10%), slices were labelled with PDF antibody (PDF C7 Hybridoma Bank 1:50, in BSA 0.25%) and probed with Vectastain Elite ABC kit followed by HRP oxidation of DAB 0.025% (Miskiewicz et al., 2008). Samples were treated for EM imaging: post-fixation (1% FA/1% GA), incubated with 1.5% ferrocyanide and OsO₄ 4% and then Thiocarbohydrazide 1%. After incubation with OsO₄ 1%, slices were incubated in Uranyl acetate 1% and then Walton Lead Aspartate. Slices were dehydrated with a series of ethanol solutions and embedded in durcupan resin (Deerinck et al., 2010). PDF labelled cells in the fly brain were approached using a serial Block-Face scanning electron microscope (Zeiss Merlin). When the first images of these cells were acquired, the sample was moved to a Focussed Ion Beam scanning electron microscope (FIB-SEM) (Zeiss Auriga) where high resolution images were acquired (Figure S5A,B) (Kremer et al., 2015). Image modelling and quantification was performed with IMOD (Kremer et al., 1996) and ImageJ software (Schneider et al., 2012). TEM images were obtained from 50 nm sections imaged on a JEM2100 [JEOL] microscope (Miskiewicz et al., 2014).

Quantitative real time PCR

Total RNA was extracted from 9-10 fly brains using the ReliaPrep™ miRNA Cell and Tissue Miniprep System (Promega). The manufacturer's protocol was followed including a DNaseI treatment to

prevent DNA contamination. Subsequently, cDNA was amplified from 1 µg of RNA using the SuperScript® III First-Strand Synthesis System for RT-PCR (Life Technologies) using a mix of oligo(dt) primers and random hexamer primers. A mock control without reverse transcriptase was included for all samples. Next, 4.5 µl of 25 ng/µl cDNA, mock or water (no template control) were loaded together with 0.5 µM of the forward and reverse primers for PDF, Parkin, Pink1, MARF or PS synthase (PSs) and the LightCycler® 480 SYBR Green I Master mix (Roche). Subsequently, the LightCycler 480 was used for analysis (Roche). Primers are listed below. The ribosomal protein RP49 was used as house-keeping gene to normalize the data for loading differences. The fold change of mRNA expression was determined for each gene using the $\Delta\text{-}\Delta\text{-CT}$ method, where the expression of the genes was compared to the control sample.

PDF_Fw	GCTCGCTACACGTACCTTGT
PDF_Rv	GATAGCGACAGAGAGTGGCC
dPark_Fw	GGAGCGTCTGAATATAACCGATG
dPark_Rv	GGATCACGATGGACAGTAAAGG
dPink1_Fw	AAGCGAGGCTTTCCCCTAC
dPink1_Rv	GCACTACATTGACCACCGATTT
MARF_Fw	GAGACGACCACCTTTATCAACG
MARF_Rv	GCCACCTTCATGTGATCCCG
PSs_Fw	TTCTACAAGCCACACACCATC
PSs_Rv	CGTTTCTGACGAACGCAAAGTA
RP-49_F	ATCGGTTACGGATCGAACAA
RP-49_R	GACAATCTCCTTGCGCTTCT

Lipid measurement in ER and mitochondrial fractions

Flies were snap frozen, heads were isolated and homogenized in buffer (Sucrose 320mM, HEPES 4mM, MgCl₂ 1.5mM, pH 7.4, with protease inhibitors) (Depner et al., 2014). Homogenate (H) was spun at 1000 g for 10 min. The supernatant (S1) was collected and spun at 13000 g for 15 min followed

by a washing step of the pellet containing the mitochondria (P2) with 1 ml of buffer. The supernatant (S2) was collected and spun at 124000 g for 1 hour to obtain a pellet enriched with ER membrane (P3). Mass spectrometry-based lipid analysis of H, P2 and P3 was performed at Lipotype GmbH as previously described (Vos et al., 2017). Ratios between the lipid amount in the ER (P3) to the amount in mitochondria (P2) are shown.

Lipid supplemented food experiment

Food supplemented with 150 μ M PtdSer or 300 μ M PtdCho (1500x the amount of these lipids in the fly food (Carvalho et al., 2012)) was prepared from the lipid stock in chloroform (25 mg/ml). The same volume of Chloroform was added in the control experiment. 1-3 days old flies were used at the beginning of each experiment.

QUANTIFICATION AND STATISTICAL ANALYSIS

Statistical Analysis

Statistical analyses were performed using GraphPad Prism 7.0 software. The criteria for significance is: ns (not significant) $p > 0.05$, * $p < 0.05$, ** $p < 0.01$, *** $p < 0.001$. Significant differences between 2 groups were analyzed using a two-tailed Mann-Whitney test. For more than 2 groups, a one-way ANOVA (with Bonferroni's post-hoc correction for multiple comparisons) was used. For the lipid supplementation analysis, a two-way ANOVA (with Tukey post-hoc correction for multiple comparisons) was used. The graph representation and error bars are defined in each legend, together with the definition of n and which statistical test was performed. Error bars show standard error of the mean (SEM), as indicated in the figure legend. Sample size was chosen according to that used for similar experiments in the literature.